U.PORTO
FEUP FACULDADE DE ENGENHARIA
UNIVERSIDADE DO PORTO

INFLUENCE OF OPERATING CONDITIONS ON THE DAMPING OF FLOATING WIND TURBINES

VÍTOR LIOTTO PEDRELLI

Dissertation sbmitted in partial fulfillment of the requirements for the degree of

MASTER OF CIVIL ENGINEERING — SPECIALIZATION IN STRUCTURES AND GEOTECHNICS

Advisor: Professor Doutor Filipe Manuel Rodrigues Leite Magalhães

Co-Advisor: Francisco Carvalho Neto de Queiros Pimenta

Supervision at VESTAS: Thea Vanelli

JULY 2023

MESTRADO EM ENGENHARIA CIVIL 2022/2023

DEPARTAMENTO DE ENGENHARIA CIVIL

Tel. +351-22-508 1901

m.ec@fe.up.pt

Editado por

FACULDADE DE ENGENHARIA DA UNIVERSIDADE DO PORTO

Rua Dr. Roberto Frias

4200-465 PORTO

Portugal

Tel. +351-22-508 1400

feup@fe.up.pt

http://www.fe.up.pt

A minha familia e amigos

“As pessoas felizes lembram o passado com gratidão, alegram-se com o presente e encaram o futuro sem medo”

Epicuro

AGRADECIMENTOS

Por mais que este seja um trabalho individual a conclusão do mesmo não seria possivel sem a participação de todos que cruzaram meu caminho durante esta longa jornada.

Nos ultimos meses passei por um dos maiores desafios que ja tive até hoje, e tenho certeza que esse trabalho não teria sido possivel sem o apoio de todos que estiveram presente direta ou indiretamente.

Gostaria de agradecer em primeiro lugar a minha irmã Amanda Liotto Pedrelli que sempre me apoiou, incentivou e foi a minha base para manter minha saúde mental. Além de sempre me ajudar com tudo que estava ao seu alcance.

Em segundo lugar, agradeço minha mãe Tatiana Liotto e meu pai Giani Pedrelli que me suportaram até nos meus piores dias, me deram espaço enquanto ainda se mostravam presentes e sempre me apoiaram da forma que podiam.

Minha família e meus amigos foram um grande pilar em que pude me apoiar durante toda esta caminhada, passamos pelos mesmos desfios e foi muito bom ter pessoas que entendem o que estamos sentindo e com o que estamos lidando.

Também serei sempre grato por todo o apoio, auxilio e conhecimentos transmitidos pelo professor orientador Filipe Manuel Rodrigues Leite Magalhães e coorientador Francisco Carvalho Neto de Queiros Pimenta, que sempre se estiveram disponiveis para qualquer ajuda necessaria me explicando tudo o tanto de vezes que fossem necessarias e sempre se mostraram interessados em aprimorar o trabalho ao maximo. Me sinto muito privilegiado por te-los como equipa de orientação.

Também agradeço a Vestas pela oportunidade de fazer parte desta grande empresa e de toda a infraestrutura que me disponibilizaram, além de todo apoio e envolvimento que tiveram durante todo o processo da dissertação, em especial a Thea Vanelli com quem passei a maior parte do tempo e que também sempre ajudou com ideias e feedbacks.

Confesso que este trabalho trouxe mais desafio do que pude imaginar, mas hoje posso afirmar que terminei este ciclo de 5 anos de estudo da melhor maneira possível, com um desafio tão grande quanto o de tomar a decisão de mudar de país para estudar fora com 18 anos de idade.

Este trabalho representa uma etapa concluida e outras que ainda estão por vir.

RESUMO

As energias renovaveis tem sido, nos ultimos anos, alvo de muita pesquisa e desenvolvimento. Dentro desta area é de grande destaque a energia proveniente dos turbinas eólicas, uma vez que estes suprem uma parcela consideravel da demanda em toda a Europa. Sendo assim, a tendência é de que se busque cada vez mais otimizar a produção atraves da implantação de mais turbinas e do aumento da capacidade de produção dos mesmos. Como também é sabido, os geradores eólicos offshore apresentam vantagem em termos de capacidade de produção, devido ao vento mais intenso e menos turbulento, porém acarreta junto a isso desafios principalmente quanto ao modelo de fundação.

Esta tese se aprofunda então em turbinas eólicas suportadas por plataformas flutuantes semi-submersíveis, sendo o principal objetivo caracterizar a influencia do vendo, correntes marítmas e o ângulo das pás no amortecimento destas estruturas.

O desenvolvimento do trabalho seguiu um planejamento bem estabelecido a priori, que consistiu em uma primeira etapa de familiarização e conceitos basicos ligados as turbinas eólicas (flutuantes) bem como seu funcionamento, seguindo então para um treinamento de utilização do software de modelação numérica “OpenFAST” (desenvolvido pelo Laboratorio Nacional de Energias Renovaveis, NREL) em paralelo com a utilização de programação para apoiar a gestão e análise dos dados.

Foram também revistos conceitos teóricos muito importantes para as respostas estruturais geradas numéricamente, mais especificamente acerca da dinâmica das estruturas, como frequencias, amortecimentos, séries temporais no dominio tempo e frequencia, entre outros.

Seguido a isso, foram estabelecidos quais parâmetros, tanto de operação quanto das ações externas, que seriam simulados. Finalmente, foram feitas as simulações em conjunto com todas as adaptações, e os resultados pós-processadas para caracterizar os parâmetros modais associados aos principais modos de vibração.

Com isso foi possivel entender principalmente a relação dos coeficientes de amortecimentos com as difentes condições ambientais que atuam sobre o sistema, e com as diferentes condições de operação de turbinas eólicas, aumentando assim a compreensão dessas estruturas tão complexas.

Palavras-Chave: Gerador eólico, amortecimento, plataforma flutuante, OpenFAST, dinâmica estrutural

ABSTRACT

Renewable energies have been the subject of much research and development in recent years. Within this area, energy from wind turbines is of great importance, since these supply a considerable portion of demand throughout Europe. Therefore, the tendency is to increasingly seek to optimize production by installing more wind turbines and increasing their production capacity. As is also known, offshore wind turbines have advantages in terms of production capacity, due to the more intense and less turbulent wind, but these also imply challenges, mainly in terms of the foundation model.

This thesis focuses on offshore wind turbines supported by semi-submersible floating platforms, being the main goal the characterization of the influence of the wind, sea currents and blade pitch on the damping of these structures.

The development of the work followed a well-established a priori planning, which consisted of a first stage of familiarization with basic concepts related to (floating) wind turbines as well as their operation, then followed by training on the use of the numerical modelling software "OpenFAST" (developed by National Renewable Energy Laboratory, NREL) in parallel with the use of programming tools to support data management and analysis.

Very important theoretical concepts for the analysis of numerically generated structural responses were also reviewed, more specifically about the dynamics of structures, such as natural frequencies, damping, time series in the time and frequency domain, among others.

Following this, the parameters, both for operation conditions and external actions, that would be simulated were established. Finally, the simulations were carried out and the outputs post-processed to characterize the modal parameters associated with the main vibration modes.

With this, it was possible to understand mainly the correlation between the damping ratios and the different environmental conditions that act on the system, and with the different operating conditions of a wind turbines, increasing in this way the understanding of these very complex structures.

Keywords: Wind turbine, damping, floating platform, OpenFAST, structural dynamics

Index

1
INTRODUCTION

1.1. BACKGROUND

In today's context, it is evident the importance of energy to societies working and progress. Nonetheless, where we can obtain energy from is also a concern, with the population growth and the technology advance the need of energy also increases, but it is well known that the fossil energy is a limited energy source with significant environmental impact. That is why renewable energies are progressively becoming more and more explored, researched, and being implemented. Regarding wind energy, it already meets 15% of Europe's demand, and in some countries even more. The International Energy Agency (IEA) expects wind to be the main power source in Europe by 2027.

Therefore, with all this potential it is expected that the technology involved in wind turbines fabrication develops as much as their structural dimensions, that is why structural analysis become more important and needed.

Other point to emphasize is that 80% of the wind resources in Europe are in water depths higher than 60 meters. The exploration of this resource brings new challenges while also having advantages. Deep waters are usually at a high distance from shore where there are steadier winds, high mean wind speeds and lower turbulence intensity, besides less visual and noise impacts, and a lot of space available. The main challenge is related with support structure design, being the adoption of floaters a promising solution.

Although allowing the exploration of higher water depths, the floater solution aggregates more degrees of freedom to the structures complicating their analysis and adding a really important component that is the sea states.

Several studies have already been carried out around onshore wind turbines, and in recent years offshore wind turbines have also been explored more and more. However, most investigations revolve around different numerical models to analyze the dynamic behavior of floating wind turbines, considering damping and its influence on the stability and performance of these systems (Jonkman, J.M., 2009).

There are also researches that focus on investigating different control strategies to improve the performance and stability of floating wind turbines, with damping being considered an important parameter in the analyzed control strategies (Savenije, Feike & Peeringa, Johan., 2014).

There are still several other studies in which damping is considered an important parameter for the development of research. And this is what the objective of this thesis is, above all, to study how different environmental conditions affect damping and estimate them for different scenarios.

1.2. OBJECTIVES

The main objective of this thesis is to study and understand the effect that different environmental and operational parameters generate in the damping of the structure motions associated with the main vibration modes.

The analysis is fully based on numerical simulations performed over a reference wind turbine model supported by a semi-submersible floating platform. The evaluation of the damping ratios is obtained from simulated free decays, motivated by initial conditions that enhance the contribution of the particular mode to be analyzed in each simulation.

The main parameters to be explored in the simulations are wind speed, sea current speeds and blade pitch angles.

The analysis is focused on the platform rigid body motions and on the main vibration modes of the tower.

1.3. DOCUMENT ORGANIZATION

The document is organized in six chapters, including this introductory chapter.

The second chapter introduces all the components that make up the wind turbine and describes how these machines operate, together with a brief description of the software that was used to run the simulations and their different modeling options.

The third chapter explains the theory of structural dynamics followed by some practical examples, but its main point is to expose and explain the method used to estimate the damping ratios from the simulated time series.

The fourth chapter, in turn, describes some specific properties of the wind turbine and platform chosen for the simulations and also shows some of the chosen simulation options. Finally, it also includes a last section that exposes the reference values for the modal properties under analysis, which will be used to understand the impact that the different simulated parameters have on the structure.

The fifth chapter explores the modal properties evolution across different environmental and operation conditions. It begins by explaining the different parameters adopted in each of the simulations and the different criteria used to estimate the modal properties, and finally, the most relevant results.

There is also a sixth chapter in which the conclusions are discussed, together with some suggestions for work that may be developed following the work developed so far.

2
FLOATING WIND TURBINES

2.1. INTRODUCTION

In this chapter, some technical aspects regarding the wind turbines will be discussed. The first part describes the most relevant components and how they work. The second part is about the simulation software that is going to be used, and how it is possible to include all the turbine properties, platform characteristics and other parameters that will be manipulated in the developed studies.

2.2. WORKING PRINCIPLES

First step to understand how a wind turbine operates is to get to know their components. Although there are a lot of different configurations for wind turbines, currently the most adopted ones for power generation are generators with horizontal axis of rotation and rotors turned to the wind direction (upwind). Also, as this thesis focus on floating wind turbines, it is this type that will be detailed in the following paragraphs.

This chapter is based on reference books such as the book written by Erich Hau (Hau, 2006), and also information collected in institutions such as EERE (Energy Efficiency & Renewable Energy).

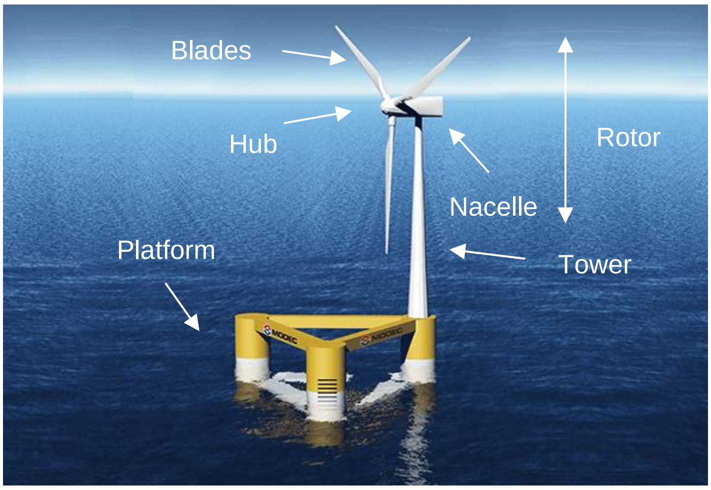

Figure 2.1 - Offshore horizontal axis generator upwind (https://www.modec.com/business/newbiz/offshorewind.html)

The main components of wind turbines are the foundation (onshore), platform (offshore), tower, nacelle and rotor, as shown in Figure 2.1. The nacelle is composed by a series of mechanical and electrical elements that can convert kinetic energy into electricity through a shaft system, that will be discussed later. The rotor is mainly formed by the blades and the hub (center where the blades are fixed) and it is through the air resistance and aerodynamic behavior of the blades that the wind will force them to spin, converting the wind energy in kinetic energy of rotation which in turn will become electricity.

The most recent wind generators are equipped with a system known as SCADA (Supervisory Control and Data Acquisition system). This system allows the operational control and monitors a series of environmental and operational parameters, such as wind speed and direction, generator speed, active power, blade pitch, nacelle orientation, rotor speed, and more.

At the top of each turbine there is a wind vane that identifies the wind direction and transmits it to the yaw drive, so it can orient the turbine to the proper wind direction. The anemometer is also located in the tower top, it quantifies the wind speed and transmits this data to the controller system. With this information, the turbine can rotate on the tower to look toward the wind direction, so the blades can create the maximum resistance against the wind.

Most wind turbines have three blades, and since the blades capture the wind energy, they have a well-defined aerodynamic shape in order to improve the capacity of extraction. The transversal section is very complex and varies along the length, these sections are known as airfoils. This shape allows that when the wind flows across the blades it creates a differential pression on each side of the blade, and generates drag and lift forces, as the lift is the stronger one it causes the rotor to spin.

Besides the aerodynamic importance, the blades also have the resistance component, so the physics and mechanical characteristics must guarantee both operational conditions and cyclic movements throughout lifetime. These should be as light as possible to avoid additional loads to the remaining structure, but also stiff enough to prevent efficiency losses and tower strikes. With all that in mind, the most used materials are composites that include glass and carbon fibers.

The nacelle is located at the top of the tower and is composed by several mechanical and electric components, as shown in Figure 2.2, that can convert the mechanical energy that come from the rotor into electricity. For most common generators, the nacelle has two shaft systems, the main one (the rotor axes) spins with the hub in a low speed (low-speed shaft) transmitting the torque to the secondary shaft (high-speed shaft) through the gearbox. This process is necessary so that the shaft rotational speed can match the generator rotational speed, making the conversion of kinetic energy into electrical energy more efficient.

In addition, there are other operating mechanisms in the nacelle. There is a mechanical brake that allows to interrupt the operation of the turbine in emergency situations. The yaw system, that rotates the nacelle on upwind turbines in order to ensure it is facing the wind, in case the wind direction changes.

There is also the pitch system that adjusts the angle of the wind turbine blades, and at the same time controls the rotor speed. This angle is critical to ensure that the turbine is extracting the greatest amount of energy possible while controlling the loads that will be transmitted to the tower. It is also possible that the angle is such that it does not cause the rotor to spin for the wind scenario below the cut-in wind speed and to slow the turbine’s rotor for high wind speed like the values above the cut-out wind speeds (which might be harmful and cause damage to the structure).

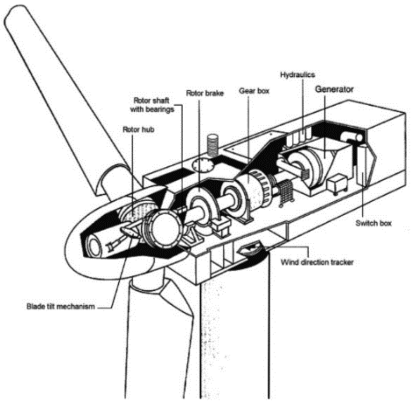

Figure 2.2 – Nacelle components (Wagner, H.-J. 2013)

Foundations for onshore wind generators are based on well-known concepts that have already been extensively explored in civil engineering, with two main solutions: slab foundations (direct foundations) or pile foundations (indirect foundations).

Slab foundations are used when the soil close to the surface is of sufficient quality to support the expected loads. In this type of solution, the moments at the base are compensated by the eccentricity of the reaction, while the vertical loads are distributed over the foundation area and the horizontal loads are balanced by the friction developed on the soil-foundation interaction surface. This solution consists of a reinforced concrete slab that generally has a polygonal geometry and variable thickness.

Pile foundations are used for soils of lower quality, or those with insufficient quality to meet the necessary requirements. They also consist of a reinforced concrete slab from which a certain number of piles extend until a soil layer of sufficient quality is reached. For this case, all loads are absorbed by the soil through the lateral and/or tip resistance of the piles.

Offshore solutions are quite diverse and complex, depending mainly on the maritime conditions of each location, in particular its depth. In this way, it is possible to classify the water depth in three categories: shallow waters, transitional waters, and deep waters. The most appropriate solutions for each category are presented in the following Table 2.1.

Table 2.1 – Foundation type recommended by water depth

Shallow waters (0 m – 30 m)	Transitional waters (30 m – 60 m)	Deep waters (h > 60 m)
• Gravity based foundation • Monopile	• Tripod Foundation • Jacket • Triple foundation	• Floating

There are three main classifications of floating wind structures (James and Ros, 2015), shown in Figure 2.3.

Semi-submersible platform: buoyancy stabilized platform which floats semi-submerged on the surface of the ocean whilst anchored to the seabed with catenary mooring lines. Often requires a large and heavy structure to maintain stability, but a low draft allows for simpler installation.

Spar-buoy: a cylindrical ballast-stabilized structure which gains its stability from having the centre of gravity lower in the water than the centre of buoyancy. Thus, while the lower parts of the structure are heavy, the upper parts are usually lighter, thereby lowering the centre of gravity with regard the centre of buoyancy. The simple structure of the spar-buoy is typically fairly easy to fabricate and provides good stability, but the large draft requirement can create logistical challenges during assembly, transportation, and installation, and can constrain deployment to waters >100m depth.

Tension leg platform (TLP): a semi-submerged buoyant structure, anchored to the seabed with tensioned mooring lines, which provide stability. The shallow draft and tension stability allows for a smaller and lighter structure, but this design increases stresses on the tendon and anchor system. There are also challenges with the installation process and increased operational risks if a tendon fails.

There are also variants of the previous typologies, such as multi-turbine floating platforms (large semi-submersible floating platforms that can support more than one turbine) and hybrid wind/wave devices (platforms that have a wind turbine and a production of energy through waves). Comparing the basic principles of stability presented, it is not possible to identify the concept that guarantees the best solution. On the one hand, each typology has its own strengths and weaknesses, presented in Table 2.2, on the other hand, the specific conditions of each location dictate these same advantages and disadvantages.

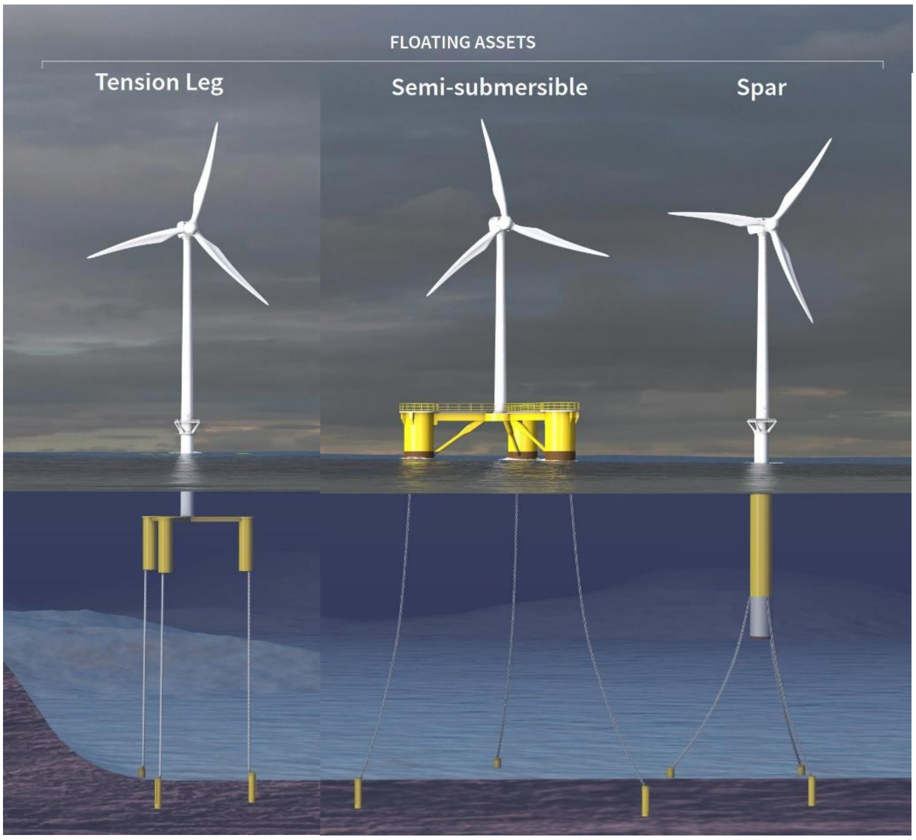

Figure 2.3 - Floating wind foundation typologies

(https://acteon.com/blog/floating-wind-mooring-options/)

Table 2.2 - Advantages and disadvantages of each of the main types of floating foundations for offshore wind generators

Typology	Strengths	Weaknesses
Semi-submersible	• Flexible application due to the ability to operate in shallow water depths • Low vessel requirement – only basic tug boats required • Onshore turbine assembly • Amenable to port-side major repairs	• High structural mass to provide sufficient buoyancy and stability • Complex steel structures with many welded joints can be difficult to fabricate • Potentially costly active ballast systems
Spar-buoy	• Simple design is amenable to serial fabrication processes • Few moving parts (no active ballast required) • Excellent stability	• Constrained to deep water locations • Offshore turbine assembly requires dynamic positioning vessels and heavy-lift cranes • Large draft limits ability to tow the structure back to port for major repairs
Tension leg platform	• Low structural mass • Onshore turbine assembly • Few moving parts (no active ballast required) • Excellent stability	• High loads on the mooring and anchoring system • Challenging installation process • Bespoke installation barge often required
Multi-turbine platform	• Net reduction in structural mass per turbine • Platform can be used to site auxiliary equipment and facilities	• Wake effects can reduce yield • Large platform could be susceptible to higher bending loads • Large platform can cause fabrication and installation challenges
Hybrid wind/wave	• Merging wind and wave technologies can reduce intermittency of supply and increase total power output	• Challenge to integrate two energy generation systems • Increased floater motion can increase turbine loads • High structural mass

2.3. NUMERICAL MODELING

The software that was used for all the simulations is OpenFAST, which is an open-source software developed by NREL (National Renewable Energy Laboratory), and was based on FAST (Fatigue, Aerodynamics, Structures and Turbulence), mostly developed and supported by Jason Jonkman, PhD (Jonkman, J. M., 2009). The software has a modular structure, as illustrated in Figure 2.5.

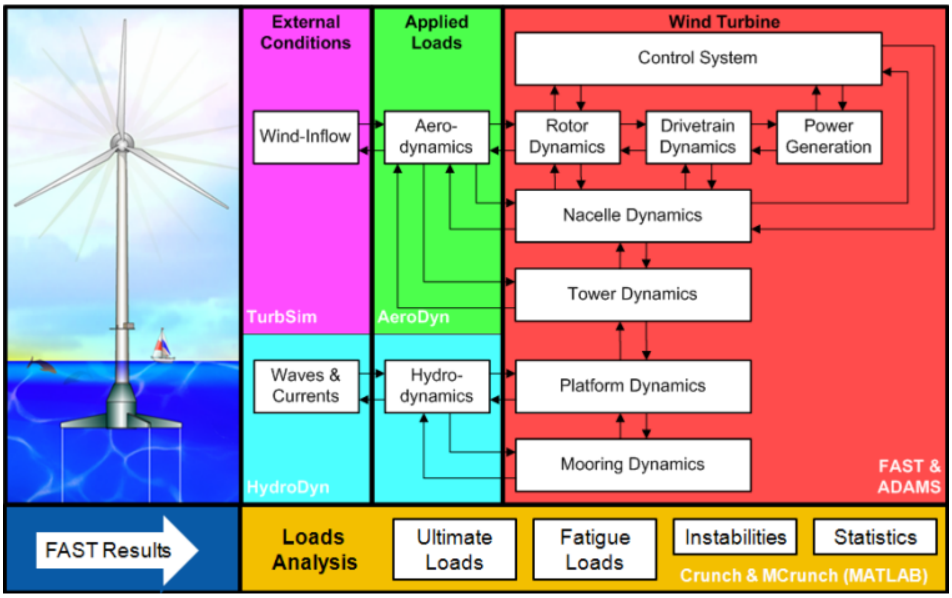

Figure 2.5 - OpenFAST Modules (Matha, Denis., 2009)

OpenFAST being an open-source software, is highly customizable, and can be adjusted to encompass every wind turbine model and platform typology. It is possible to define specific initial conditions, external loads, different operation criteria, control options, among others.

Firstly, it is very important to explain and introduce the degrees of freedom that are taken into account in this type of structures. For the tower, its deformation is characterized considering the contribution of a pair of mode shapes, in both perpendicular directions and located in the tower top, called fore-aft (FA) and side-side (SS) (as depicted in Figure 2.6).

For the platform, movements are characterized by means of six degrees of freedom: three translations (surge, sway, heave) and three rotations (roll, pitch, yaw). The translations and rotations listed are movements, respectively, on the x, y, z axes, considering that the wind direction is in the x axis, the y axis also horizontal and perpendicular to the same wind direction and finally, the z axis is vertical.

Aditionally there are other two degrees of freedom to characterize each blade deformation, being called flapwise and edgewise (directions in Figure 2.6).

Finally other degree of freedom that has to be mentioned is the nacelle yaw system, that allows the nacelle to rotate in relation to the tower, looking towards the wind direction.

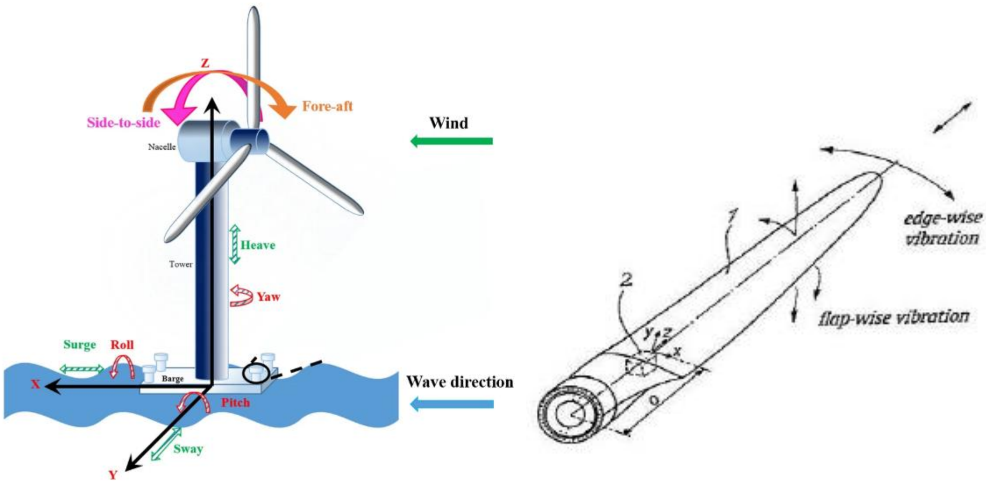

Figure 2.6 – Tower degrees of freedom (Ahmad, I., 2023) (left) and blade degrees of freedom (Tartibu, 2015) (right)

For each simulation, it is necessary to specify which modules are going to be used, as well as the module file path.

Each module deals with specific characteristics, and in the next paragraphs the functions and options of each of these modules will be detailed and explained.

All the information adopted to describe the following modules was obtained through the information provided by Jonkman, J. M., 2005 and also in the main repository for the NREL-supported OpenFAST whole-turbine and FAST.Farm wind farm simulation codes, accessed via openfast.readthedocs.io.

Starting with ElastoDyn, this module contains multiple features, such as, which degrees of freedom will be considered in the simulations, which initial conditions are desired (blade pitch angle and rotor speed), the turbine configuration that indicates information such as number of blades, tower height, mass and inertia distribution of the system, gear box properties, beside others.

It also includes the indication of the file path that leads to complementary files that will be used, two of the main ones are the file containing the properties of each of the blades, and the file containing the properties of the tower, such as stiffness, mass and mode shapes to be considered.

There is also a section to choose which variables will be shown in the output file. These can be displacements and accelerations at the top of the tower and/or on the floating platform (if applicable), rotor rotation speed, among many others.

Furthermore, it also defines the turbine configuration, such as, rotor principal angles, overall dimensions (rotor radius and tower height) and the rigid bodies (hub and nacelle) center of mass position, total mass and inertia.

InflowWind is a module for generating wind series that allow the aeroelastic simulation of wind turbines.

In this module, it is possible to define the wind properties that will act on the structure. There are different wind models that can be used for this.

The three most commonly used models can generate: steady, uniform winds and a third type which is generated by a software called TurbSim (not included in OpenFAST) that applies a statistical model to numerically build time series of wind speed vectors. These vectors are three-dimensional and are located at the nodes of a vertical, two-dimensional grid.

The latter is the most recommended, as it is possible to include factors such as turbulence, which makes the simulation more realistic.

But, since the purpose of this thesis is to evaluate the effects caused by specific conditions, the model that will be used considers steady winds, thus allowing to obtain simpler response time series that facilitate the interpretation of the results.

In this steady model, it is possible to define the wind speed, wind propagation direction, upflow angle, reference height for the horizontal wind speed, and the power law exponent to define wind speed variations as a function of the height.

Wind turbine control and safety systems are defined in the ServoDyn module. This module allows the control of specific turbine operating conditions in several ways. In total, there are five basic control systems implemented: pitch control, generator moment control, generator shaft brake, rotor shaft brake and nacelle orientation. Each of the mentioned systems can be defined according to several methods. The simplest control methods only require the configuration of some parameters in the main input file. More complex control methods require algorithms to be built, compiled, and integrated into the software.

However, in the context of the present work, in order to study the impacts of the different evaluated parameters, it is necessary that these remain constant throughout the duration of the simulation. That is, once defined, for example, a blade pitch, it must be kept constant throughout the simulation, as well as the rotor speed.

The aerodynamic forces that act on the structure, more precisely on the blades and the tower, are determined in AeroDyn. This module calculates the aerodynamic loads at the blade and tower nodes and returns them back to OpenFAST.

The primary AeroDyn input file defines modeling options, environmental conditions (except freestream flow), airfoils, tower nodal discretization and properties, tower, hub, and nacelle properties, as well as output file specifications. Airfoil data properties are included in dedicated input files (one for each airfoil), with coefficients for estimation of lift and drag forces. Blade nodal discretization, geometry, twist, chord and airfoil identifier properties are likewise read from separate input files (one for each blade).

HydroDyn is the FAST module responsible for quantifying the hydrodynamic loads on the substructure, fundamental in the numerical simulation of offshore wind generators (floating or fixed). This module is coupled to OpenFAST, however it can also be activated as an independent code to calculate the hydrodynamic loads.

HydroDyn allows several approaches for calculating the hydrodynamic loads acting on the structure, a solution based on potential flow theory, a solution based on strip theory (Journee and Adegeest, 2003) or an hybrid combination of the two previous solutions.

Regarding the simulation of the maritime conditions to be analyzed, this module allows defining the environmental conditions (water density and water depth), whether or not there are waves in the simulation, as well as their properties, such as significant wave height of incident waves, lower and upper frequency limit of the wave spectrum, incident wave propagation heading direction, range of wave directions, among others.

HydroDyn's standard current model includes three sub-models: near-surface, sub-surface, and depth-independent, as illustrated in Figure 2.7. All three currents are vector summed, along with the wave particle kinematics velocity.

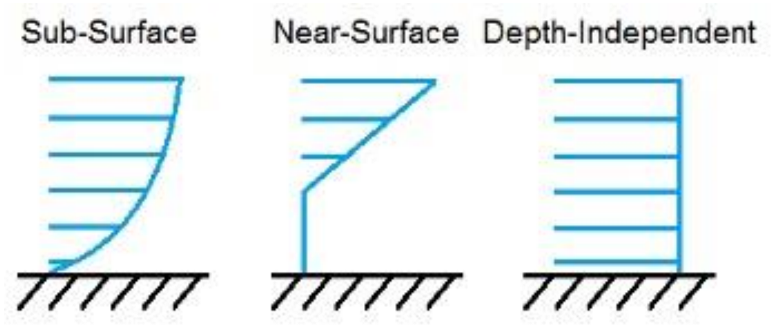

Figure 2.7 - Standard Current Sub-Models (OpenFAST)

When coupled to OpenFAST, HydroDyn receives as input data and at every instant the position, orientation, velocities, and accelerations of the various nodes of the substructure (rigid or flexible), from which it calculates the hydrodynamic loads. It should be noted that the ElastoDyn module considers the substructure of the floating platforms as a rigid body with six degrees of freedom. For the fixed offshore solutions, the SubDyn module allows simulating the structural flexibility of multi-membered substructures, thus coupling hydrodynamic and elastic effects.

SubDyn is a module of structural dynamics in the time domain, aimed at calculating the substructure of fixed bottom (non-floating) offshore wind turbines. The type of substructures supported by this module are: monopile, tripile, jacket and other truss-type substructures (Figure 2.8), common in offshore wind installations in shallow and transitional water depths. SubDyn can also be used to model supporting structures for onshore wind generators, such as steel lattice towers.

As in this thesis the focus will be on semi-submersible, this module will not be used in the simulations.

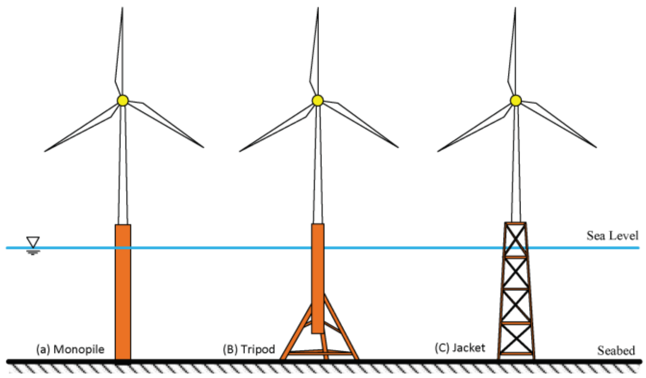

Figure 2.8 – Fixed bottom foundation types (Plodpradit, P., 2019)

The MoorDyn module models the structural behavior of the mooring lines of offshore wind solutions. This module allows to consider mooring systems with multiple configurations, mooring lines with variable properties, arbitrary connections between lines, and even floats and weights concentrates (clump weights). In the evaluation of the structural behavior, it is possible to model the contact of the lines with the seabed, the friction of the seabed and the external forces. And like most modules, there is also the alternative of resorting to external software.

The last two modules are designed to model the interaction between non-floating offshore wind generators and the presence of surface ice.

IceFloe was created by DNV GL and includes the option to apply loads following various models for monopile type structures or multi-leg structures with the same diameter. For structures of support with multiple legs, the ice loads are calculated independently for each of them, however, factors that simulate the shadow effect can be considered.

IceDyn was developed by the University of Michigan and includes six ice mechanical loading models that incorporate the impact of ice masses, structural deformation and failure, and geometry. The six models are: static loading on vertical structures, dynamic loading on vertical structures, random ice loads on vertical structures, non-uniform loading on vertical structures, ice loads on inclined structures, and impact of large masses of ice.

It is important to note that this was just a brief introduction to the modules present in OpenFAST and some of the options available for different simulation situations. Some of these options had to be chosen for the development of this thesis and will be discussed in Chapter 4.

3
DYNAMICS OF FLOATING WIND TURBINES

3.1. INTRODUCTION

In this chapter the mathematical formulations that explain the dynamic behaviour of structures will be discussed. Firstly, the concepts of damped and undamped responses will be presented, as well as linear and nonlinear behaviour. In addition, simple examples that help to visualize and understand the concepts under analysis will be presented.

It is known that all structures vibrate, but to guarantee that the amplitude of these vibration are not detrimental to the structure, dissipation of energy performs an important role. The amount of dissipation, known as damping, can vary a lot, but it is always present in all structures. It will control the vibration level and thereby, it can affect the lifetime of the structure. Damping is influenced both by the intrinsic characteristics of the structure, as well as by the environmental conditions to which the structure will be subject. In the case of floating wind turbines two factors that play a significant role in damping are the movement of the structure through its surrounding media, air or water, or a combination of both. Because many sources cause dissipation in a vibrating system, it is difficult to model them individually. This is one of the difficulties that had to be overcome throughout the works developed and that will be explored throughout the remaining of this chapter.

3.2. EQUATIONS OF MOTION

The primary objective of a structural-dynamic analysis is the evaluation of the displacements over time of a given structure subject to a given time-varying load. The mathematical expressions defining the dynamic displacements are called the equations of motion of the structure, and the solution to these provides the required displacement time-histories.

To formulate these equations of motion there are some different approaches that can be used. The one that will be presented and used in this thesis is d'Alembert's principle, that is the one based on Newton's second law of motion.

A discrete system is a system that can be described through the motion of a discrete number of points **i**, $(u_i(t), v_i(t), w_i(t))$. To each function $f_i(t)$ that characterizes the movement of a point in one direction, there is one degree of freedom. This system opposes the continuous systems whose movement is described through continuous functions in the systems points, $(u(x, y, z, t), v(x, y, z, t), w(x, y, z, t))$, i.e. continuous functions in the time and space of the structure.

A discrete system of a single degree of freedom (SDOF) is a system that beyond discrete, its movements are described by only one point in one direction i.e., through just one function $f(t)$.

Considering the system of Figure 3.1, the equation of motion can be easily formulated by just using d'Alembert's principle to express the equilibrium of all forces acting on the system. The forces applied to the system in the degree of freedom direction are the external applied force p(t) and the inertia, damping and stiffness forces: $f_I(t)$, $f_D(t)$ and $f_S(t)$. The equilibrium of these forces represents the equation of motion:

$$f_I(t) + f_D(t) + f_S(t) = p(t) \tag{3.1}$$

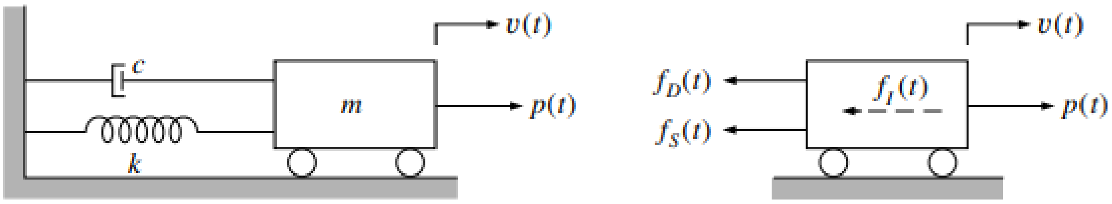

Figure 3.1 - Discrete System of SDOF

The first resisting force is the inertia force $f_I(t)$ that according to d'Alembert's principle is the product of the mass and acceleration:

$$f_I(t) = m \cdot \ddot{u}(t) \tag{3.2}$$

Assuming by now a viscous damping mechanism, the second resisting force is the damping force $f_D(t)$ which is given by the product of the damping constant c and the velocity:

$$f_D(t) = c \cdot \dot{u}(t) \tag{3.3}$$

Lastly, the third resisting force is the elastic force $f_S(t)$ which is given by the product of the stiffness and displacement:

$$f_S(t) = k \cdot u(t) \tag{3.4}$$

When the equations are merged the equation of motion for this system is given by:

$$m \cdot \ddot{u}(t) + c \cdot \dot{u}(t) + k \cdot u(t) = p(t) \tag{3.5}$$

Although as mentioned before this equation is considering a viscous damping mechanism, there are other kinds of damping that can be considered, such as the aerodynamic and hydrodynamic damping.

When an aerofoil (such as a blade) moves relative to the air, it generates an aerodynamic force in a rearward direction, at an angle determined by the direction of relative motion. This aerodynamic force is commonly resolved into two components, both acting at the centre of pressure.

Drag is the force component parallel to the direction of relative motion, and is given by the following expression:

$$F_d = \frac{1}{2} \cdot \rho \cdot u^2 \cdot C_d \cdot A \tag{3.6}$$

Lift is the force component perpendicular to the direction of relative motion, and is given by:

$$F_l = \frac{1}{2} \cdot \rho \cdot u^2 \cdot C_l \cdot A \tag{3.7}$$

Where ρ is the air density C_d and C_l are, respectively, the drag and lift coefficients and A is the blade section area. Figure 3.2 illustrates these two forces.

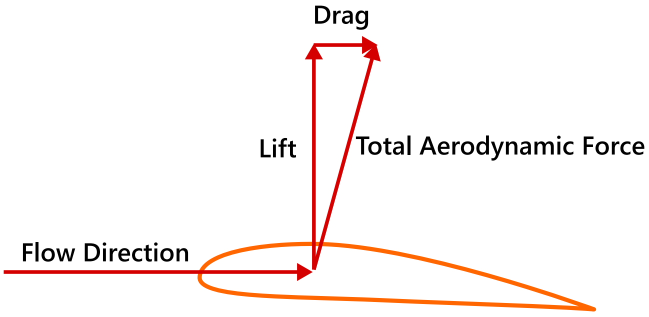

Figure 3.2 -Aerodynamic Forces on a blade (Wikimedia Commons, 2023*)*

Because of the dependence of a force on the squared velocity, it is also possible to instead of having an equation of motion with a damping force with a proportional dependence on the velocity, to have a dependence to the squared of the velocity, what would result in a different formulation, such as:

$$m \cdot \ddot{u} + c \cdot \dot{u} \cdot |\dot{u}| + k \cdot u = p(t) \tag{3.8}$$

The modulus of the velocity is used to ensure that the force and the velocity have opposite directions.

For the hydrodynamic force something very similar happens.

Besides that, these equations are written in the time domain, but there is other way to represent it, in frequency domain, for which it is necessary to apply the Fourier Transform (FT). The Fourier Transform converts a signal from the time domain to the frequency domain by decomposing it into its harmonic components. This allows the identification of the frequencies that compose the signal, as well as their respective amplitudes and phases (see Figure 3.3).

The mathematical expression responsible for this transformation is given by:

$$F(\omega) = \int_{-\infty}^{\infty} f(t) \cdot e^{-i\cdot\omega\cdot t}\, dt \tag{3.9}$$

Where the Fourier transform response is composed of a portion of real and imaginary numbers, with amplitude and phase.

The process starts with a random time waveform. The algorithm takes frames of equal length and applies the FFT (Fast Fourier Transform) to each frame. Then, it calculates the squared magnitude for each frequency bin and finds the average. The mean-square value is the "power" of the quantity and measurement of signal strength.

Finally, the algorithm divides the mean-square value by the bandwidth to normalize it.

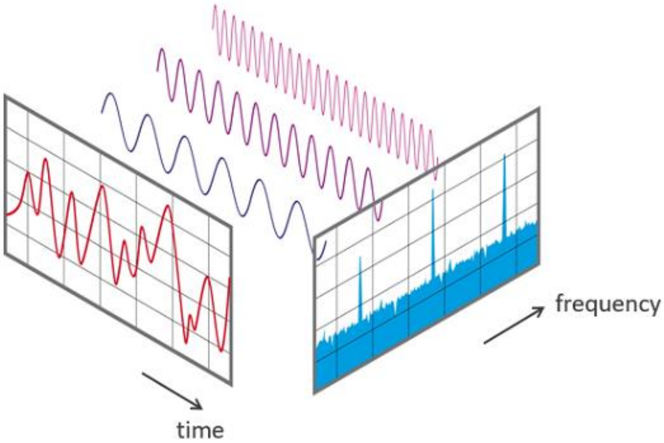

Figure 3.3 – Time vs frequency domain

(https://www.nti-audio.com/en/support/know-how/fast-fourier-transform-fft)

If the FFT is applied to equation 3.5, it results in the following equation, in frequency domain [Hz].

Assuming that:

$$u(t) \;\rightarrow\; \tilde{u}(\omega) \tag{3.10}$$

$$\dot{u}(t) \;\rightarrow\; i \cdot \omega \cdot \tilde{u}(\omega) \tag{3.11}$$

$$\ddot{u}(t) \;\rightarrow -\omega^2 \cdot \tilde{u}(\omega) \tag{3.12}$$

That when replacing, leads to:

$$-m \cdot \omega^2 \cdot \tilde{u} + c \cdot i \cdot \omega \cdot \tilde{u} + k \cdot \tilde{u} = \tilde{p} \tag{3.13}$$

Being:

$$\tilde{u} = \frac{1}{k + c \cdot i \cdot \omega - m \cdot \omega^2} \cdot \tilde{p} \tag{3.14}$$

Where the first component of the product is the frequency dependency due to the structural part and the second is due to the external loads.

3.3. Motion of 1DOF System

3.3.1. Linear damping force

The essential physical properties of any linearly elastic structural or mechanical system subjected to an external source of excitation or dynamic loading are its mass, elastic properties (flexibility or stiffness), and energy-loss mechanism or damping. In the simplest model of a SDOF system, each of these properties is assumed to be concentrated in a single physical element (Figure 3.1).

The movement of free vibration of an undamped 1DOF system is obtained by solving equation 3.5, but disregarding the external load and the damping parcel, remaining:

$$m \cdot \ddot{u}(t) + k \cdot u(t) = 0 \tag{3.15}$$

That has the general solution:

$$u(t) = A \cdot cos\,(w \cdot t) + B \cdot sin\,(w \cdot t) \tag{3.16}$$

The replacement of this solution will result in imposing the relation:

$$w = \sqrt{\frac{k}{m}} \tag{3.17}$$

Where **w [rad/s]** is designated angular frequency and it can be noted that the solution is a periodic function of period **T [s]** or frequency **f [Hz]**:

$$u(t+T) = u(t) \quad \rightarrow \quad w \cdot (t+T) - w \cdot t = 2 \cdot \pi \tag{3.18}$$

$$T = \frac{2 \cdot \pi}{w} \quad \leftrightarrow \quad f = \frac{1}{T} = \frac{w}{2 \cdot \pi} \tag{3.19}$$

Through the initial conditions, the displacement, and the velocity at the instant **t = 0s**, it is possible to determine the constants **A** and **B**.

The undamped system will have a behaviour shown in the Figure 3.4.

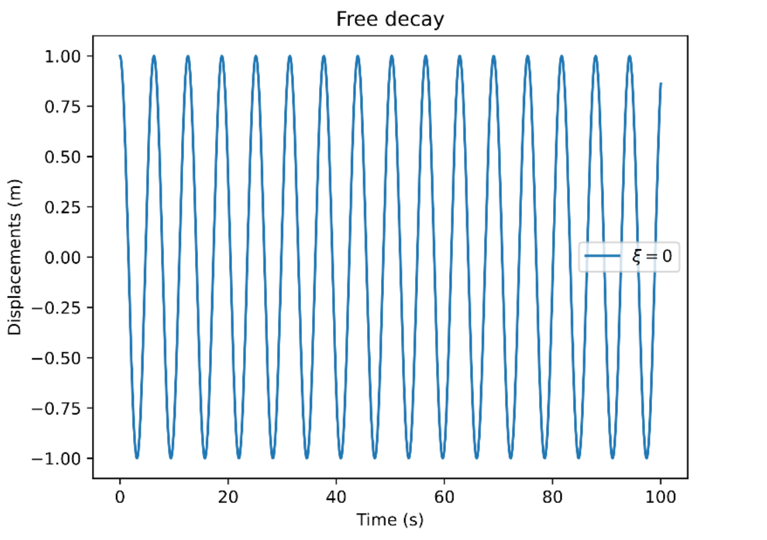

Figure 3.4 – Undamped free decay

Assuming now a damped one degree of freedom system, the structural response in obtained by solving the following equation:

$$m \cdot \ddot{u}(t) + c \cdot \dot{u}(t) + k \cdot u(t) = 0 \tag{3.20}$$

This has two solutions:

$$u(t) = C \cdot e^{s_1 \cdot t} \quad \wedge \quad u(t) = C \cdot e^{s_2 \cdot t} \tag{3.21}$$

$$s_1 = -\frac{c}{2 \cdot m} + \sqrt{\left(\frac{c}{2 \cdot m}\right)^2 - \frac{k}{m}} \quad \wedge \quad s_2 = -\frac{c}{2 \cdot m} - \sqrt{\left(\frac{c}{2 \cdot m}\right)^2 - \frac{k}{m}} \tag{3.22}$$

Being, this way, the general solution the sum of both:

$$u(t) = C_1 \cdot e^{s_1 \cdot t} + C_2 \cdot e^{s_2 \cdot t} \tag{3.23}$$

For cases where the damping is less than the critical one, a damping coefficient is defined:

$$\xi = \frac{c}{c_{cr}} = \frac{c}{2 \cdot m \cdot w} < 1 \tag{3.24}$$

In this case the general solution is:

$$u(t) = C_1 \cdot e^{-\xi \cdot w \cdot t + i \cdot w_a \cdot t} + C_2 \cdot e^{-\xi \cdot w \cdot t - i \cdot w_a \cdot t} \quad (3.25)$$

$$u(t) = e^{-\xi \cdot w \cdot t} \cdot (A \cdot cos\,(w_a \cdot t) + B \cdot sin\,(w_a \cdot t)) \quad (3.26)$$

Being the $w_a = w * \sqrt{1-\xi^2}$ the angular frequency of the damped system. Using this definition, the two solutions for the equation 3.23 can be rewritten as:

$$u(t) = C \cdot e^{s_1 \cdot t} \quad \wedge \quad u(t) = C \cdot e^{s_2 \cdot t} \quad (3.27)$$

$$s_1 = -\xi \cdot w + i \cdot w \cdot \sqrt{1-\xi^2} \quad \wedge \quad s_2 = -\xi \cdot w - i \cdot w \cdot \sqrt{1-\xi^2} \quad (3.28)$$

$$s_1 = -\xi \cdot w + i \cdot w_a \quad \wedge \quad s_2 = -\xi \cdot w - i \cdot w_a \quad (3.29)$$

Equation 3.26 is a periodic function modulated by an exponential function and is represented for different damping ratios in Figures 3.5 to 3.7.

From the initial condition (displacement and velocity at the instant **t = 0s**), it is possible to determine the value of the constants **A** and **B**.

Note that it is possible to get the maximum envelope using only the first part of equation 3.26:

$$me(t) = e^{-\xi \cdot \omega \cdot t} \cdot A \quad (3.30)$$

For a controlled application example, the first step is the calculation of a structural response time series that goes from **t = 0s** to **100s** spaced by **0.01s**. From there, it was used the equation of the general solution, for linear damped free vibration structures (equation 3.26).

After defining the equation (3.26), the next step is to define the parameters, amplitudes **A [m]** and **B [m]**, damping ratio **ξ [%]** and frequency **f [Hz]**. After defining the frequency, it is possible to immediately get the value for the angular frequency **ω [rad/s]** through equation 3.19. Then with all the parameters chosen, it is possible to plot the equation of the general solution defined in equation 3.30 that represents the free decay along the time. And finally, from that it is possible to get the maximum envelope, resulting into the following examples:

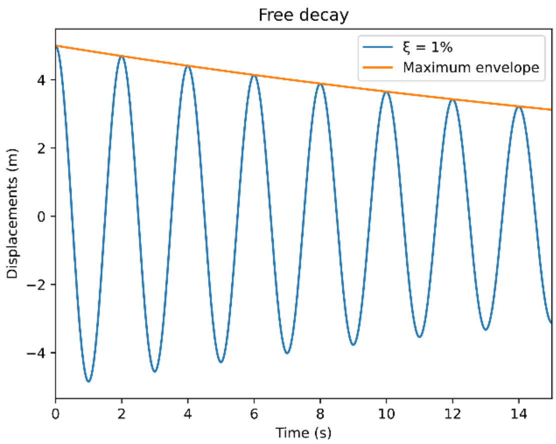

Figure 3.5 – Free decay with 1% damping

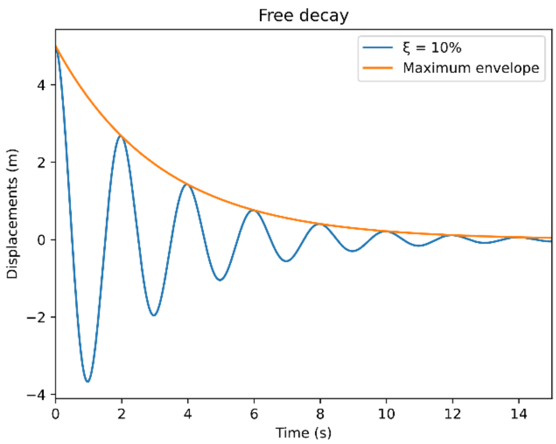

Figure 3.6 – Free decay with 10% damping

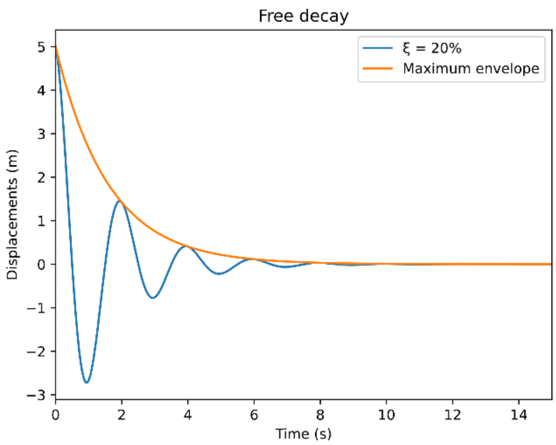

Figure 3.7 – Free decay with 20% damping

The three images presented have all the same amplitudes A = 5m and B = 0m, frequency f = 0.5 Hz and consequently the same angular frequency ω = 2 * π * f rad/s, but there are different values for the assumed linear damping coefficient, that are represented in order by the following damping ratios $\xi = \{0.01; 0.10; 0.20\}$.

Now, applying the Fourier Transform to the time series of the previous graphs, it is possible to plot them in frequency domain. These plots are presented in Figures 3.8 to 3.10. Note that the amplitude in the y axis is represented in a logarithmic scale.

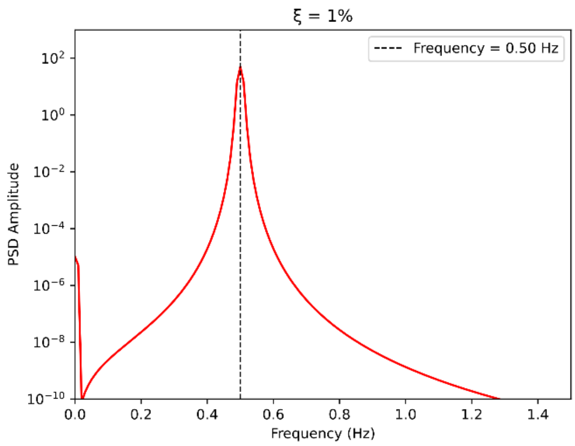

Figure 3.8 – Spectrum of free decay with 1% damping

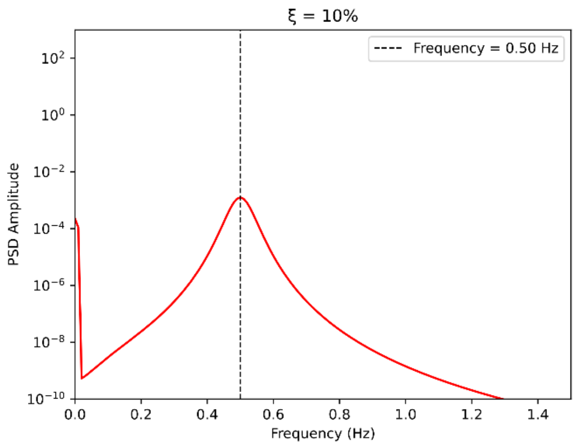

Figure 3.9 – Spectrum of free decay with 10% damping

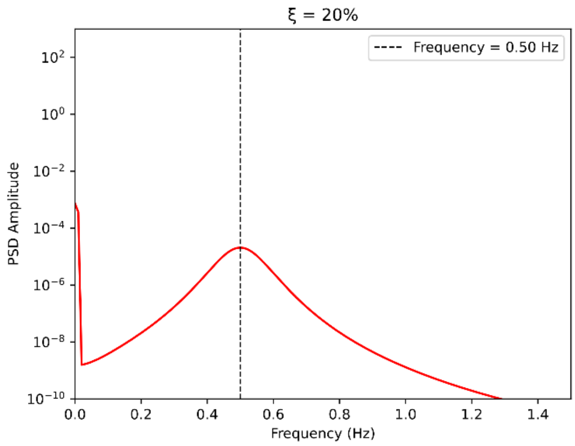

Figure 3.10 – Spectrum of free decay with 20% damping

Note that with increasing damping the peaks for a frequency of 0.5 Hz decrease in absolute value (y axis), which means that there is less energy in the movement, since the greater the damping is the greater is also the energy dissipation. It is also noted that the width of the peak increases and it ceases to be so slender and pointed and becomes more flattened.

In Figure 3.11 it is possible to make a direct comparison between the spectra associated with the three different values of damping.

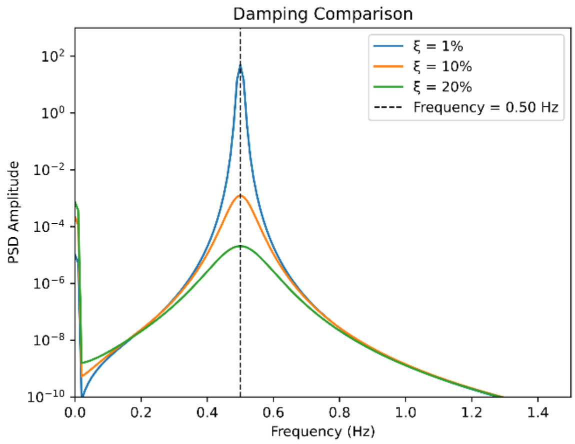

Figure 3.11 – Spectra of all free decays with different damping ratios

3.3.2. Non-linear damping force

In addition to the cases in which damping follows a linear law, there are cases in which it follows a non-linear law, as discussed in section 3.2.

Taking into account aerodynamic or hydrodynamic forces, it would result in a formulation such as:

$$m \cdot \ddot{u} + c \cdot \dot{u} \cdot |\dot{u}| + k \cdot u = 0 \qquad (3.31)$$

For this type of equation, it results a free decay as presented in Figure 3.12.

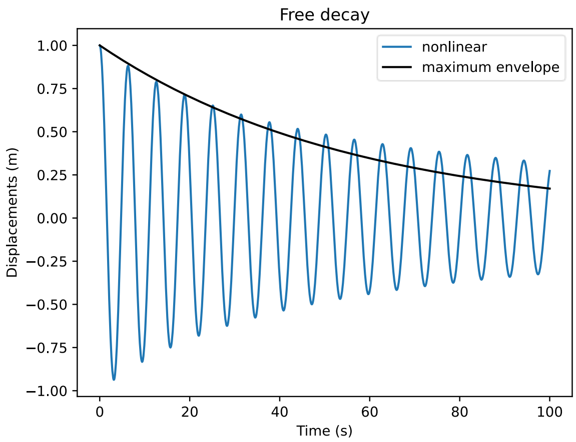

Figure 3.12 – Nonlinear damping free decay and maximum envelope of a linear damping decay

This output is very similar to the linear equation case (Eq. 3.26), but in the section 3.4 of this chapter the differences will be clarified.

In reality, considering the contribution of a structural damping and aerodynamic and hydrodynamic damping there is an overlapping of the linear and nonlinear components to represent the behaviour of the system. Because of this, the damping force will be a sum of the two contributions.

$$m \cdot \ddot{u} + c_0 \cdot \dot{u} + c_1 \cdot \dot{u} \cdot |\dot{u}| + k \cdot u = 0 \tag{3.32}$$

In this case, it is taken into account that the free decay energy dissipation would have a portion that has a linear dependence and other that has a nonlinear dependence. In addition, for situations where there are high relative velocities with regard air or water, the portion that will have the greatest influence on damping will be one with the coefficient $\mathbf{c_1}$, as the velocity decreases, the greatest contribution becomes the one with the coefficient $\mathbf{c_0}$.

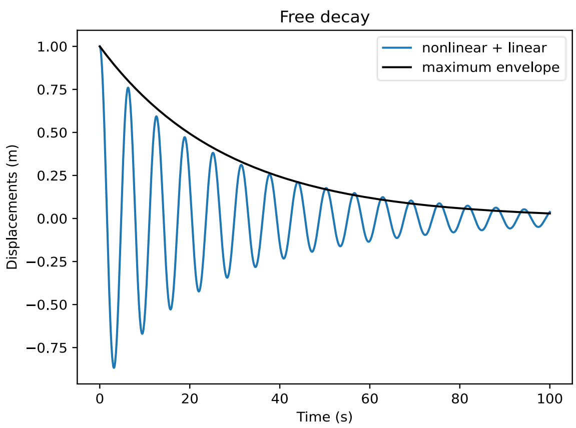

Figure 3.13 – Nonlinear + linear damping free decay and maximum envelope of a linear damping decay

In this case, it is also difficult to identify the differences between the linear model and this nonlinear one, but in Figure 3.14 there is a graph with the three models together for a direct comparison.

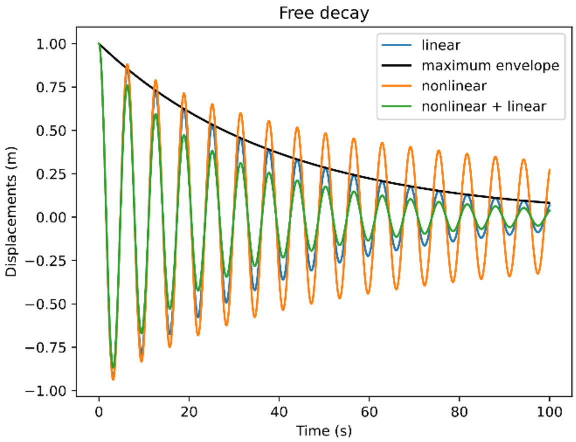

Figure 3.14 – All damping cases free decays

Note that all the cases previously presented (linear, nonlinear and nonlinear + linear) have the same parameters values, both **m** and **k** have unit values, either **c** or $\mathbf{c_0}$ or $\mathbf{c_1}$ are equal to **0.025**, in consistent units (si), and note that the only case where the exponential maximum envelope fits is for the linear model.

3.4. Experimental estimation of modal damping ratio

Since wind turbines are very complex structures, the damping coefficient is correlated with many different factors. For example, each part of the structure (tower, platform, mooring cables) has different stiffness, inertia, and gravity centre, in addition to being conditioned by the external conditions to which the structure is subject. This ends up making it impossible to arrive at a single model capable of representing the free decays, since it would be necessary a different model/equation for each degree of freedom in each of the external conditions imposed.

However, it would be unfeasible to mathematically deduce a different solution for each simulation. Therefore, the method that will be used to estimate damping will be described in the next paragraphs. This thesis will use a method that is based in the equations presented before. It is easy to notice, in Figure 3.15, that the maximum envelope cannot be represented by the first method, presented in Eq. 3.30. This image is from a real simulation of a free decay from an imposed initial displacement of 10m in the floating platform of a wind turbine in the surge direction (no wind, no wave).

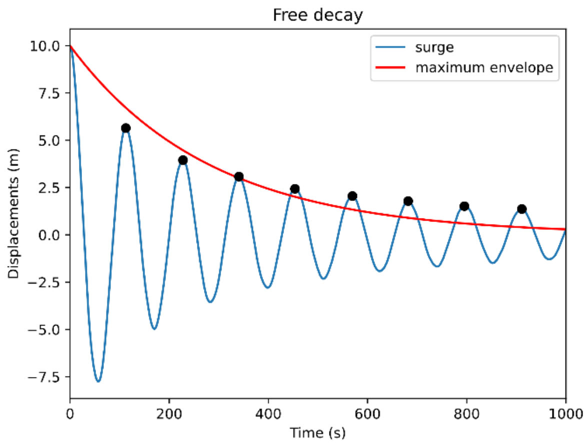

Figure 3.15 – Free decay of a simulation example

One way to overcome this situation is to represent the free decay amplitude evolution on time, but in a natural logarithmic scale, then grouping the maxima three by three and fitting a linear trendline to the envelope of these maxima. As the points are represented in a natural logarithmic scale, the output from the linear trendline is going to be the exponent of equation 3.30, but expressed in a linear function given by y = a * t + b.

This was the maxima envelope used before

$$me(t) = e^{-\xi \cdot \omega \cdot t} \cdot A \tag{3.33}$$

Appling natural logarithmic to both sides

$$ln\,(me(t)) = ln\,(e^{-\xi \cdot \omega \cdot t} \cdot A) \tag{3.34}$$

$$ln\,\big(me(t)\big) = -\xi \cdot \omega \cdot t + ln\,(A) = a \cdot t + b \tag{3.35}$$

Finally, it is possible to get the damping ratio simply by dividing **a** by the angular frequency **ω**, since **b** is only used to adjust the initial coordinate in y axis.

$$\xi = -\frac{a}{\omega} \tag{3.36}$$

With all these steps and doing it for every three maximum points (two periods) it will result into different values of damping ratios depending on which group is being considered.

In order to compare the results from all the simulations, it is necessary to adopt some criteria that will be used for all the sets of simulations. All the simulations have an initial displacement imposed (movement amplitude), which is going to be called **A**, but since the damping ratio is calculated from sets of three points (one before and one after) the first maximum does not have a previous value to compose a group of three, so the first damping ratio value is calculated for the second maximum, and this point will have an amplitude of movement called $\mathbf{A_2}$, that amplitude will be associated with a damping value that will be called $\boldsymbol{\xi_2}$. As the end of the simulation can be a little bit polluted the last maximum value used is the one that has a value greater than or equal to 5% of the initial amplitude **A** and will be called $\mathbf{A_1}$ ($\mathbf{A_1 \geq 0.05 * A}$), which also has a damping associated that will be denominated $\boldsymbol{\xi_1}$ (see Figure 3.16)

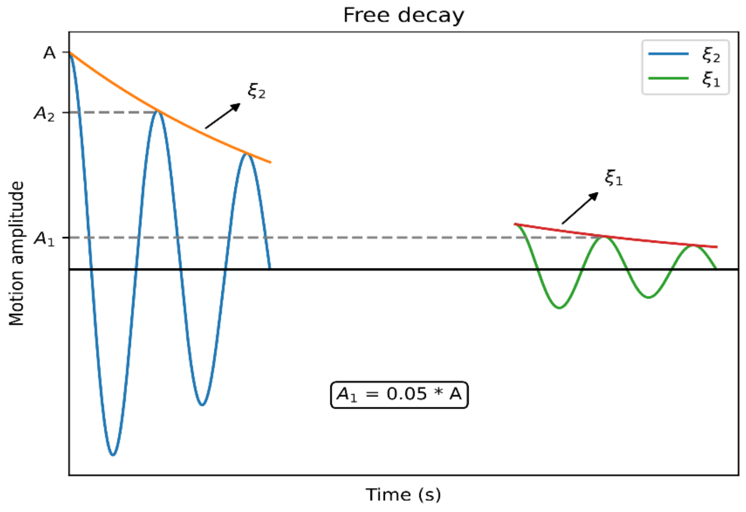

Figure 3.16 – Method for evaluation of damping ratios exemplified

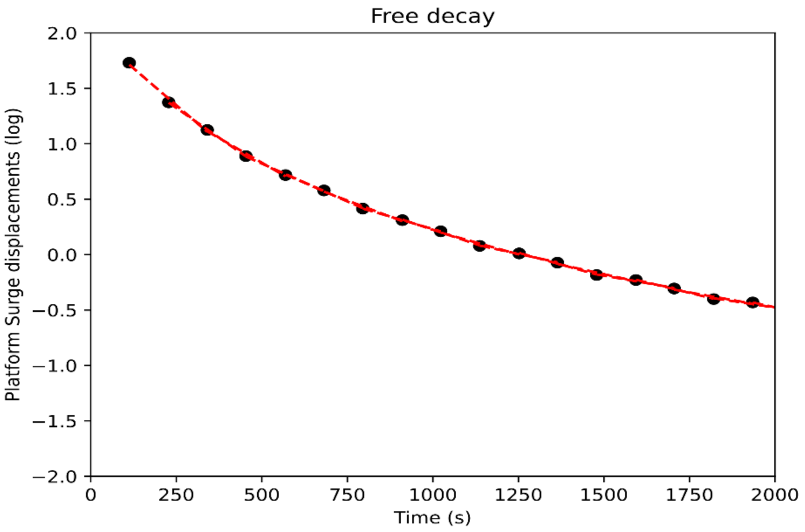

Figure 3.17 – Method for evaluating the maxima envelope

Now it is possible to have a “maximum envelope (by sections)” that fit all the local maxima (see Figure 3.17).

From that it is possible to obtain and plot the damping ratio of each group of three points. It can either be plotted in a graph of **ξ [%] x Time [s]** or a graph of **ξ [%] x Amplitude [m or º]**.

Since the considered metric of the damping ratio, in some cases, may have a dependence on the amplitude of the movement (the larger the amplitude is the larger the damping ratio will be), the damping ξ_2 will be the highest one and ξ_1 will be the lowest. But it is also possible to fit a linear trending line to the damping values and extrapolate it until it crosses the y axis where it will show the value of the damping for an amplitude of zero, which will be called ξ_0. From that trending line, it is also possible to get the coefficient (**m**) that represents the growth of the estimated damping ratio with increasing amplitude.

The value of ξ_0 represents the damping ratios associated with the linear component. While the $\mathbf{m}_\xi$ represents the damping ratios associated with the nonlinear component. So, the following equation might be written:

$$\xi(A) = \xi_0 + m_\xi \cdot A \tag{3.37}$$

3.5. Analysis of simple case studies

To illustrate the methodology described in Section 3.4, the time series generated in section 3.3 were used as input. Figure 3.18 presents the results for one of the linear cases (Equation 3.5), where the time series have also been included. As it was expected, the value of the damping ratio remains the same for all the motion amplitudes, because the **mξ** is almost equal to zero which means that there is any nonlinear contribution.

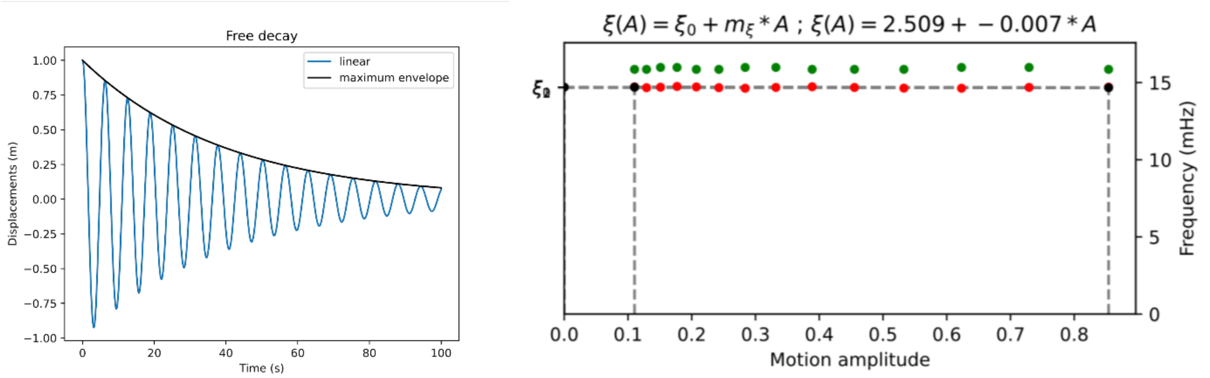

Figure 3.18 – Routine for only linear contribution (green – frequencies; red – damping ratios)

Figure 3.19 show the results for the case with nonlinear damping. It also makes sense once the ξ_0 is equal to zero, which means that there is no linear contribution, but instead of that, now the $\mathbf{m}_\xi$ is different from zero and shows a value that is consistent with the **c** associated to a nonlinear damping.

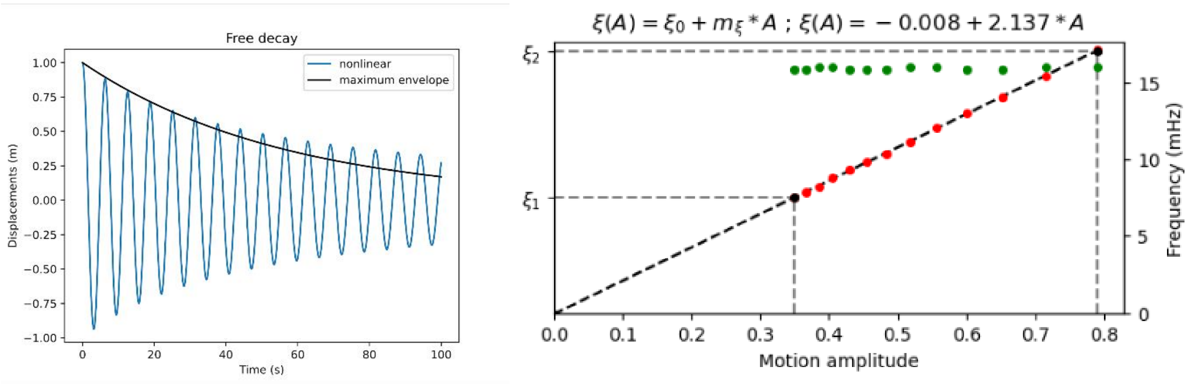

Figure 3.19 – Results for the example with only nonlinear contribution

And finally, the results for a more realistic case, where there are both linear and non-linear contributions, are represented in Figure 3.20. In the case both **ξ0** and **mξ** are different from zero.

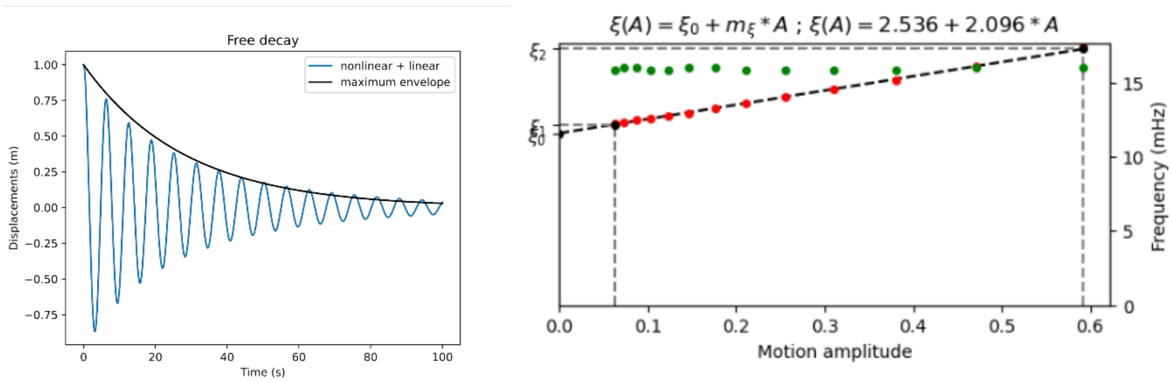

Figure 3.20 – Results for example of both linear and nonlinear damping contributions

4

CASE STUDY AND METHODOLOGY VALIDATION

4.1. INTRODUCTION

In this chapter, the properties of the tower and platform used in the simulations will be characterized. Then, it will be described how the structure was modelled in the adopted software.

Finally, the values of the modal properties that will be used as a reference for future comparisons in chapter 5 will be exposed.

4.2. STRUCTURE DESCRIPTION

This section of the thesis describes some particular characteristics of the wind turbine used in the simulations and is written based on the technical report NREL/TR-500-38060 by NREL (National Renewable Energy Laboratory), “Definition of a 5-MW Reference Wind Turbine for Offshore System Development”, written by JM, Jonkman & Butterfield, S. & Musial, W. & Scott, G. It also includes the properties of the semisubmersible floating system described in “Definition of the Semisubmersible Floating System for Phase II of OC4” written by A. Robertson, J. Jonkman, M. Masciola, and H. Song.

The referred document for the wind turbine characteristics contains specifications of a representative utility-scale multi-megawatt turbine now known as the “NREL offshore 5-MW baseline wind turbine”. The model is a conventional three-bladed upwind, variable-speed, variable blade-pitch-to-feather-controlled turbine and has been, and most likely will continue to be, used by diverse research teams around the world to standardize baseline offshore wind turbine specifications.

For the purpose of this work, only some specific characteristics of the turbine used in the simulations will be discussed.

The properties of the tower for the NREL offshore 5-MW baseline wind turbine will depend on the type of support structure used to carry the rotor-nacelle assembly. The type of support structure will, in turn, depend on the installation site, whose properties vary significantly through differences in water depth, soil type, and wind and wave severity. Offshore support-structure types include fixed-bottom monopiles, gravity bases, and spaceframes (such as tripods, quadpods, and lattice frames) and floating structures. This section documents the tower properties for the equivalent land-based version of the NREL 5-MW baseline wind turbine.

The semisubmersible floating platform is composed of three main columns that guarantee the buoyancy, and an additional central column that supports the wind generator. At the base of each main column there are plates that ensure greater dynamic stability, increasing damping and reducing vibrations induced by the waves and the operation of the generator. In the lower section of the columns there is a static water ballast system, which places the platform at the operating height.

Figure 4.1 shows the tower and the platform.

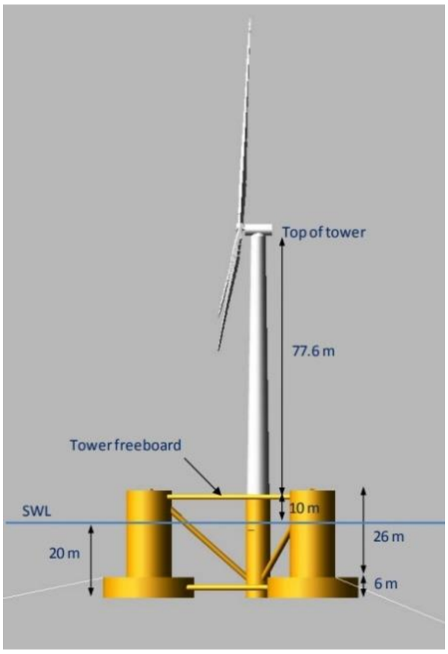

Figure 4.1 – Tower and platform main dimensions (NREL/TR-500-38060)

Details of the floating platform structure are provided in Figure 4.2 and Figure 4.3. The draft of the platform is 20 m. The tower is cantilevered at an elevation of 10 m above the SWL (sea water level) to the top of the main column (MC) of the floating platform. Between the top and bottom of the platform, the OC4 DeepCwind semisubmersible consists of a main column attached to the tower and three offset columns that are connected to the main column through a series of smaller diameter pontoons and cross members.

The mass, including ballast, of the floating platform is 1.3473E+7 kg. This mass was calculated such that the combined weight of the rotor-nacelle assembly, tower, and floating platform, plus the weight of the mooring system (not including the small portion resting on the seafloor) in water balances with the buoyancy (i.e., weight of the displaced fluid) of the undisplaced platform in still water. The CM (centre of mass) of the floating platform, which includes everything except the tower, rotor-nacelle assembly, and moorings, is located at 13.46 m along the platform centreline below the SWL. This value was set so that the overall system CM matched that of the scale-model DeepCwind system. The roll and pitch inertias of the floating platform about its CM are both 6.827E+9 kg-m^2 about the platform x-axis and y-axis respectively, and the yaw inertia of the floating platform about its centreline is 1.226E+10 kg-m^2.

Table 4.1 shows some of the floating platform properties.

Figure 4.2 – As-built picture of DeepCwind semisubmersible for 1/50th scale tests (OC4) (NREL/TR-500-38060)

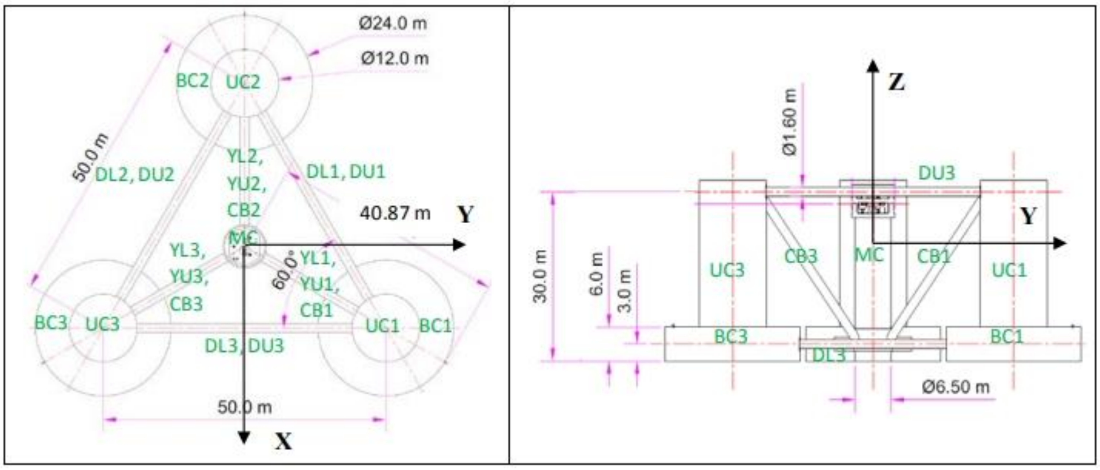

Figure 4.3 – Platform geometry (NREL/TR-500-38060)

Table 4.1 – Floating platform geometry

Depth of platform base below SWL (total draft)	20 m
Elevation of main column (tower base) above SWL	10 m
Spacing between offset columns	50 m
Length of upper columns	26 m
Length of base columns	6 m

To secure the platform, the OC4-DeepCwind semisubmersible is moored with three catenary lines spread symmetrically about the platform Z-axis. The mooring layout in the basin is shown in Figure 4.4. The mooring line properties are listed in Table 4.2. The fairleads (body-fixed locations where the mooring lines attach to the platform) are located at the top of the base columns at a depth of 14.0 m below the SWL and at a radius of 40.87 m from the platform centreline. The anchors (fixed to the inertia frame) are located at a water depth of 200 m below the SWL and at a radius of 837.6 m from the platform centreline. One of the lines is directed along the negative X-axis (in the XZ-plane). The two remaining lines are distributed uniformly around the platform, such that each line, fairlead and anchor, is 120º apart when looking from above, as shown in Figure 4.4. These properties are relative to the undisplaced position of the platform. Each of the three lines has an unstretched length of 835.5 m, a diameter of 0.0766 m, an equivalent mass per unit length of 113.35 kg/m, an equivalent apparent mass in fluid per unit length of 108.63 kg/m, and an equivalent extensional stiffness of 753.6 MN. Drag and added mass of the mooring lines due both to hydrodynamic loading and seabed interaction will be modelled using the coefficients provided in Table 4.2, which summarizes all of the mooring properties.

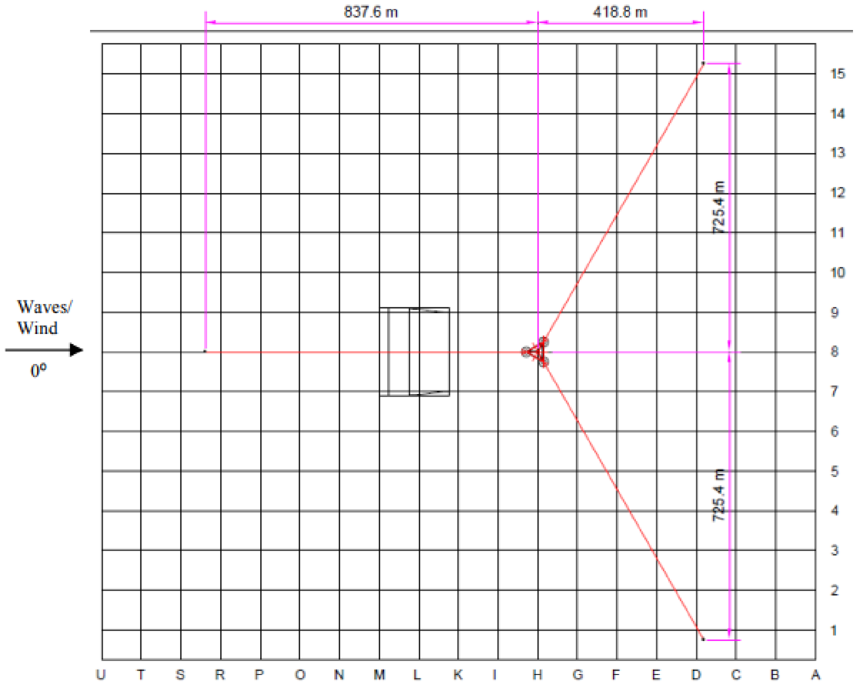

Figure 4.4 - Mooring line arrangement (NREL/TR-500-38060)

Table 4.2 - Mooring System Properties

Number of Mooring Lines	3
Angle Between Adjacent Lines	120 º
Depth to Anchors Below SWL	200 m
Radius to Anchors from Platform Centreline	837.6 m
Unstretched Mooring Line Length	835.5 m
Mooring Line Diameter	0.0766 m
Equivalent Mooring Line Mass Density	113.35 kg/m
Equivalent Mooring Line Mass in Water	108.63 kg/m
Equivalent Mooring Line Extensional Stiffness	753.6 MN
Hydrodynamic Drag Coefficient for Mooring Lines	1.1
Hydrodynamic Added-Mass Coefficient for Mooring Lines	1.0
Seabed Drag Coefficient for Mooring Lines	1.0
Structural Damping of Mooring Lines	2.0 %

The base of the tower is coincident with the top of the centre column of the floating platform and is at an elevation of 10 m above the still water level (SWL). The top of the tower is coincident with the yaw bearing and is located at an elevation of 87.6 m above the SWL. This tower-top elevation is the same as the land-based version of the NREL 5-MW baseline wind turbine. Note that these properties are all relative to the undisplaced position of the platform.

DeepCwind semisubmersible are founded on the base diameter of 6.5 m, which matches the diameter of the main column of the semisubmersible (see Figure 4.3), and the tower-base thickness (0.027 m), top diameter (3.87 m) and thickness (0.019 m). The Young's modulus was taken to be 210 GPa, the shear modulus was taken to be 80.8 GPa, and the effective density of the steel was taken to be 8.500 kg/m3. The 8.500 kg/m3 density considers an addition to the typical steel value (7.850 kg/m3) to account for paint, bolts, welds, and flanges that are not included in the tower thickness data. This value is only used for the density of steel in the tower and not elsewhere in the structure. The radius and thickness of the tower are assumed to be linearly tapered from the tower base to tower top.

The resulting overall (integrated) tower mass is 249718 kg and is centred (i.e., the centre of mass [CM]) of the tower, is located at 43.4 m along the tower centreline above the SWL. This is derived from the overall tower length of 77.6 m.

A structural-damping ratio of 1% is specified for all modes of the isolated tower (cantilevered at the top of a rigid foundation without the rotor-nacelle assembly mass present), which corresponds to the values used in the DOWEC study (Kooijman, 2003).

The Tables 4.3 and 4.4 summarize relevant properties.

Table 4.3 – Tower properties

Elevation to Tower Base (Platform Top) Above SWL	10 m
Elevation to Tower Top (Yaw Bearing) Above SWL	87.6 m
Overall (Integrated) Tower Mass	249,718 kg
CM Location of Tower Above SWL Along Tower Centreline	434.4 m
Tower Structural-Damping Ratio (All Modes)	1 %

Table 4.4 – Gross Properties of the NREL 5-MW Baseline Wind Turbine

Description	Value
Rating	5 MW
Rotor position, configuration	Upwind, 3 blades
Control	Variable speed, collective pitch
Drivetrain	High speed, multiple-stage gearbox
Rotor, hub diameter	126 m, 3 m
Hub height	90 m
Cut-in, rated, cut-out wind speed	3 m/s, 11.4 m/s, 25 m/s
Cut-in, rated rotor speed	6.9 rpm, 12.1 rpm
Rated tip speed	80 m/s
Overhang, shaft tilt, precone	5 m, 5º, 2.5º
Rotor mass	110000 kg
Nacelle mass	240000 kg
Tower mass	347460 kg
Coordinate location of overall center of mass	(-0.2 m, 0.0 m, 64.0 m)

4.3. Modeling description

As mentioned in the previous section, the parameters presented here were obtained through works developed prior to the beginning of the investigations of this thesis. The parameters presented in section 4.2 (Jonkman, J.M., 2005) and the modeling that will be described (Jonkman, J.M., 2009) in this section were duly tested and validated.

The platform is modeled as a rigid body to which different hydrodynamic properties are associated based on a potential model, previously calculated (in this case from WAMIT). Viscous damping effects, absent from this model, are further included by quadratic damping matrices.

The cables are modeled with the so-called lumped-mass models, that is, they are divided into a set of masses to which mechanical and hydrodynamic properties are associated.

The tower dynamic behaviour is described by means of the first two vibration modes in each direction. The blades dynamic behaviour is described by means of 3 vibration modes, 2 in the flapwise direction and 1 in the edgewise direction.

The tower was divided into 10 equal sections and for each of these sections parameters such as mass density, stiffness, among others, were calculated. The blades were divided into 48 sections to characterize their properties and 17 blade elements were used for integration of the aerodynamic and structural forces.

It is important to highlight that given the simplified scenarios considered and the type of analysis to be carried out, the control systems were not activated directly, with the initial conditions of each simulation having been properly defined.

For each simulation it is also important to define which outputs will be needed for future analyses. The most important outputs that were included in all simulations were the platform displacements (translations and rotations) and the displacements and accelerations at the top of the tower. Values that were not used directly for the analysis were also included, but rather to validate that the simulations ran with the defined parameters, such as wind speeds, blade pitch angles and rotor rpm.

4.4. PRELIMINARY ANALYSIS

Since the main objective of this thesis is to study and understand how certain parameters affect the wind turbine, to quantify the impact and relevance that each parameter individually has in the structure, it is important to have reference base values. With that it is easier to identify, understand and even quantify these impacts.

To get these reference values, a series of simulations were performed without changing any parameter, only imposing an initial excitation on the degree of freedom under study, while the others remained without initial displacements. By doing this, it is possible to isolate and analyse the behaviour at that specific degree of freedom.

For example, to study the behaviour of the structure in the surge direction, an initial displacement of 10 meters was imposed only in this direction. From the response obtained for that perturbation, it is possible, by the methods presented in Chapter 3, to estimate the frequency corresponding to that degree of freedom, as well as to estimate the damping ratio. Figure 4.5 shows how the results were presented and analysed after applying the methods, presented in chapter 3, in the OpenFAST simulated time series.

For all these simulations and all the others that will be done, using the Python language, a set of graphs is obtained that show the results of the programmed and automated analysis of the method presented in Chapter 3.

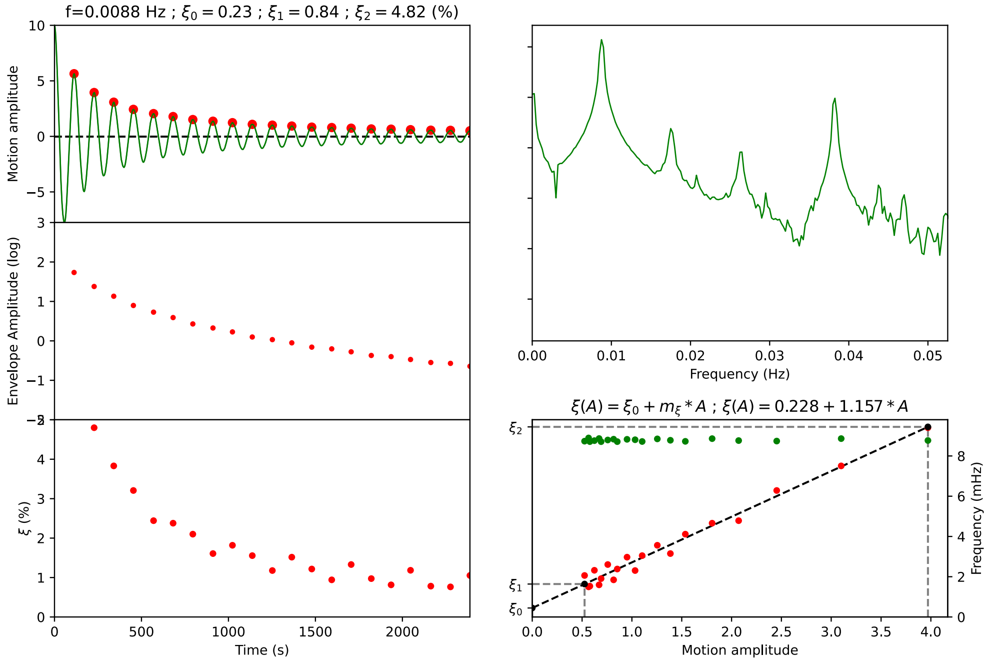

Figure 4.5 – Reference values for surge direction

In the left side there are all the graph that use the same x axis, that is the time in seconds. The first one in the top has the motion amplitude in the y axis, either in meters for the translations or in degrees for the rotations. It is basically the free decay graph. Then, bellow the first graph there is the second one, that isolates the free decay local maxima and plot them in a logarithmic scale. These points are the ones that will be used to group three by three and have a trendline to estimate damping, as already discussed in chapter 3. And finally at the bottom there are the damping ratios, each one referring to a group of three points from the graph above. That is why for the first local maximum there is no correspondent damping, because there is no point before that one to be able to group it, so the first damping ratio obtained is for the second local maximum.

Apart from that, in the top right side, there is the spectrum, that is obtained from the fast Fourier transform (FFT). In the x axis there are the frequencies in hertz [Hz] and in the y axis there are the PSD that is the power spectral density. Finally in the bottom right there are two graphs in the same plot, one in red dots that shows the motion amplitude, in the x axis, by the damping ratio, in the y axis (note that it has the same scale as the y axis of the graph in the left), and one in green which shows the evolution of the identified natural frequency.

It is possible to note that for these simulations a spectrum dominated by only one well-defined peak is obtained and with an order of magnitude much higher than any other. This is due to the fact that when forcing the motion in only one direction, it will be the mode associated to this direction that will be more relevant. This also motivates the definition of a simulation for each degree of freedom where there is a perturbation exclusively in that degree of freedom, in order to have a “cleaner” reading of the results.

It is also relevant to highlight that there is another peak (10 times smaller than the main peak, but still relevant compared to the rest) present around the frequency of 3.8E-02 Hz, which refers to the pitch motion. And in the damping ratio versus time graph, there is a sinusoidal variation, most likely due to this contribution. Taking into account the structure and the imposed motion (surge direction), it is easily justifiable since surge and pitch motions as well as sway and roll are very related.

In some cases, due to this interference from other modes, it may be necessary to apply some filter to the spectrum to "clean" the results and ensure that the analysed decay is dominated by the motion referring to the degree of freedom selected to be studied and not to any other.

In these cases, that are still to be discussed, a Butterworth filter was applied. This filter is a type of signal processing filter designed to have a frequency response that is as flat as possible in the passband, which means that for the desired frequency band there will be a negligible interference. In this filter, it is possible to indicate a lower limit to filter the frequencies, an upper limit, or both lower and upper.

In Figure 4.6, it is analysed the same simulation presented previously (surge direction), but now with a Butterworth filter applied with different parameters.

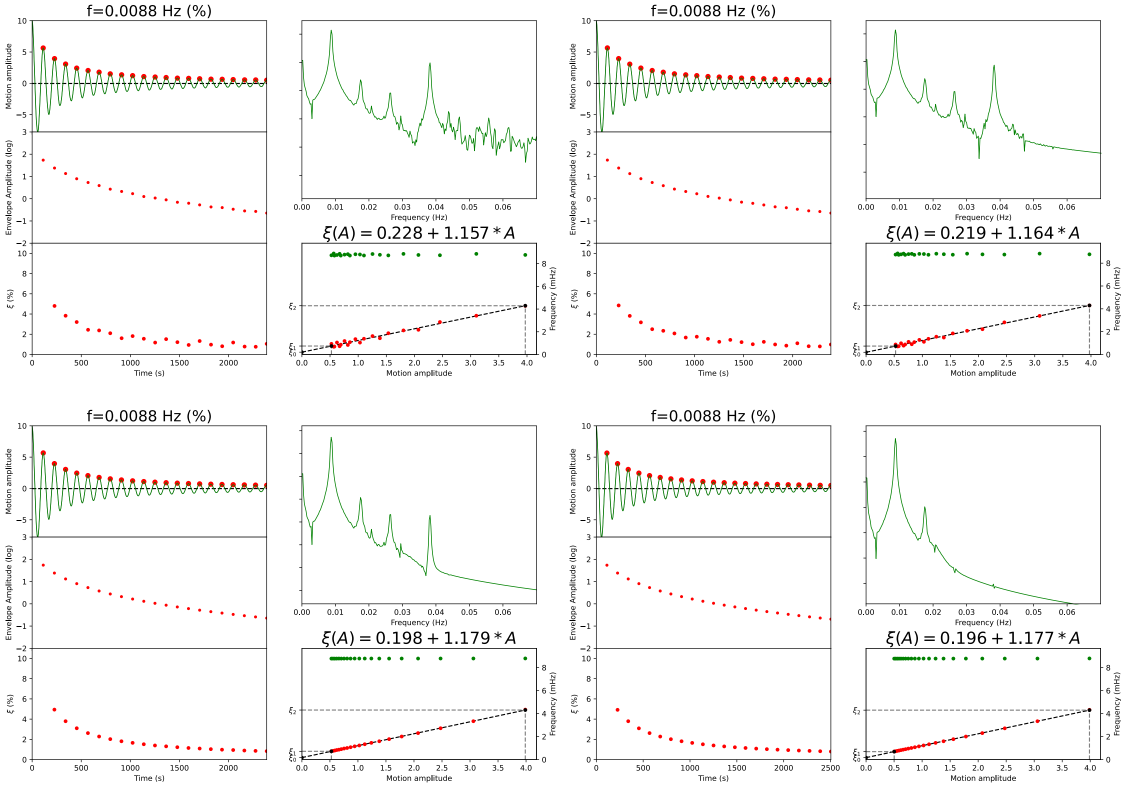

Figure 4.6 – Filter effect on spectrum: up left corner the original graph; up right a filter for frequencies above 0.04 Hz, lower left corner a filter for frequencies above 0.03 Hz, bottom right a filter for frequencies higher than 0.02 Hz

When analysing the impact that the filter has on the results, it is noticed that the more aggressive the filter is, that is, filtering closer to the frequencies it is wanted to study, the "cleaner" the results are, since the sinusoidal variation due to the participation of other modes (in this case the pitch) is filtered out and disappears. Above all, care must be taken to ensure that the defined filters are not affecting the results of the frequencies to be analysed. The figure 4.7 shows an example, for the same simulation, but for a filter of 0.0125 Hz applied, and as can be noticed, for this case the spectrum frequency that needs to be analysed have already changed its form and the results may no longer be reliable. It is in fact observed that the damping estimation changed significantly.

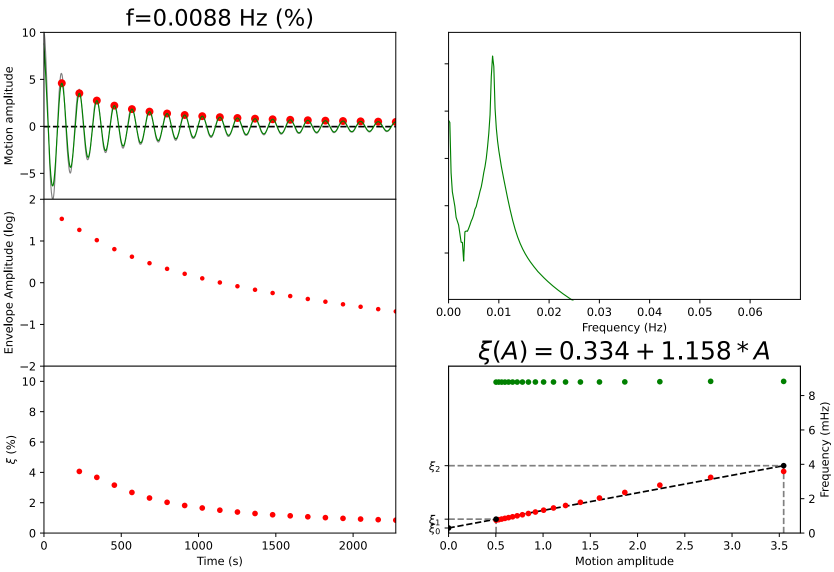

Figure 4.7 – Filter effect on spectrum (surge reference decay)

In the cases of well-tuned filters, the variation in the results is residual and that most of the time brings more reliable results than if no filter was applied, because this response only considers motions in the surge direction and not in the pitch direction, so when filtering these movements (pitch) only the movements of the surge that were intended from the beginning are left.

After analysing the surge motion, the same procedure was conducted for the remaining degrees of freedom. The amplitude of the initial displacements imposed on each degree of freedom are listed in Table 4.5 and were used both for the reference values simulations and for the simulations with different parameters that will be explored in Chapter 5.

Table 4.5 – Initial displacement imposed

Platform degree of freedom	Motion amplitude
Surge	10 meters
Sway	10 meters
Heave	2 meters
Roll	5 degrees
Pitch	5 degrees
Yaw	10 degrees
FA	1 meter
SS	1 meter

As said before from the outputs of those simulations, it was possible to estimate the frequencies and the damping ratio for each degree of freedom. And from this first set of simulations, the so-called reference results were obtained, which are presented in Table 4.6.

Table 4.6 – Reference values

Platform direction	Displacement	Frequency [Hz]	ξ_0 [%]	ξ_1 [%]	ξ_2 [%]
Surge	10 m	8.80E-03	0.23	0.84	4.82
Sway	10 m	8.80E-03	0.27	0.90	4.91
Heave	2 m	5.76E-02	0.03	0.57	4.61
Roll	5 º	3.82E-02	0.01	0.44	3.97
Pitch	5 º	3.82E-02	0.01	0.44	3.95
Yaw	10 º	1.27E-02	0.19	0.49	2.98

In these reference simulations and analysing the results alone (without comparisons) it is not possible to conclude much, but it is worth mentioning the similarities between the translation movements in the x and y axis (surge and sway) as well as the rotational movements (roll and pitch).

Considering that there are relevant differences in the natural frequencies associated with each mode, to ensure a certain uniformity, and make sure that the simulations have a similar number of cycles, or periods, 3 different durations were set up for the simulations. The table below shows the duration of each simulation.

Table 4.7 – Simulation time

Platform direction	Total simulation time [s]
Surge	4000 s
Sway	4000 s
Heave	1000 s
Roll	1000 s
Pitch	1000 s
Yaw	3000 s
FA	400 s
SS	400 s

Other two values that have a significant meaning are the $\boldsymbol{\xi_0}$ and the $\mathbf{m}_{\boldsymbol{\xi}}$ since it can indicate if the behaviour of the structure in that specific degree of freedom is better represented by a linear, nonlinear or both linear and nonlinear contribution model, as seen before in chapter 3.

Table 4.8 – Reference values

	ξ_0 [%]	m_ξ
Surge	0.228	1.157
Sway	0.269	1.175
Heave	0.030	5.321
Roll	0.015	1.641
Pitch	0.012	1.602
Yaw	0.186	0.442
FA	0.980	0.000
SS	1.350	0.000

The more the values of the damping ratios are distributed along an average value with little or no dispersion, that is, ξ_0 different from zero and m_ξ equal to or very close to zero, the closer the movement is represented by a linear model.

As the damping ratios start to be distributed along a trend line, that is, the value of m_ξ moves away from zero, the model becomes better represented by a model that has a significant nonlinear component. In particular, if the value of ξ_0 is still different from zero, there is still a linear part contributing to the movement, but if the ξ_0 is equal to or very close to zero, it means that the movement is mostly dominated by the non-linear part.

The other values (ξ_2 and ξ_1) are going to be mentioned again later, when there will be more simulations for them to be compared with.

The method was tested for the reference scenarios and very satisfactory results were obtained, which made it possible to proceed with the analysis of the remaining scenarios with different parameters, which will be presented and discussed in the next chapter.

5

INFLUENCE OF OPERATING CONDITIONS ON MODAL PROPERTIES

5.1. INTRODUCTION

The parameters and environmental conditions that were studied during this dissertation were wind speed and water current speed.

For the simulations in which there is wind, the speeds that were used are 3 m/s, 8 m/s, 11.4 m/s, 22 m/s and 30 m/s. The winds of 3 and 30 m/s are, respectively, the cut-in and above the cut-out, so for these conditions the turbine is considered parked, that is, the rotations per minute (RPM) of the rotor are 0 rpm. Note that when the wind reaches 3m/s the turbine comes out of a parked condition, so it was considered as the worst scenario, the turbine parked with a wind of 3m/s.

Furthermore, in a first phase only winds of 3, 22 and 30 m/s were studied, even though, for winds of 3 and 30, the blade pitch is not expected to be 20º, as it is wanted to study exclusively the effect of the wind, for these scenarios the blade pitch was equal to the one expected for a wind of 22m/s, which is 20º, so the blade pitch would be the same for all cases, 20º. However, with the progress of the investigations, it was decided to include two more wind speeds, 8 and 11.4 m/s, the second value referring to the rated wind speed, and the first to better characterize the behaviour from the beginning of operation (cut -in) up to the rated. In short, it is added the rated and another point between the cut-in and rated wind speeds.

For these two new wind speeds, the value of the blade pitch is 0º, maximizing the extraction of energy from the wind. For wind speeds above 11.4 m/s, the blade pitch starts to increase to keep the rotor rpm at its maximum capacity, until, for speeds above the cut-out, it returns to 0 rpm. For winds of 8 and 11.4 m/s, the rotor rpm values are 9.2 and 12.1, respectively.

Also aiming to understand the effect caused by the blade pitch, a scenario was simulated in which all conditions would be the same, except for the blade pitch. For this purpose, a wind of 30 m/s was chosen and, in addition to the simulation with a blade pitch of 20º, another one with a 90º pitch was added.

The Table 5.1 shows the operating conditions that were taken into account during the simulations for the different wind scenarios.

Table 5.1 – Simulation conditions

Wind speed	Blade Pitch	RPM	Generator
3 m/s	20 º	0	Off
8 m/s	0 º	9.2	On
11.4 m/s	0 º	12.1	On
22 m/s	20 º	12.1	On
30 m/s	20 º	0	Off
30 m/s	90 º	0	Off

For the simulations in which the water currents effect were studied, the current values used were 0.25 m/s, 0.50 m/s, 0.75 m/s and 1.00 m/s. The values used were selected from records obtained by IPMA (Portuguese Institute for Sea and Atmosphere, I. P.), that is a public institution. On the website it is possible to read Ocean forecast model NEMO (http://www.nemo-ocean.eu/) developed by the consortium CMCC, CNRS, INGV, Mercator Ocean, NERC-Met Office. From the records and forecasts, the values that are studied in this thesis were selected.

For all these simulations, no wind speed was included, as well as for the wind simulations, no water currents were included. In this way, it is possible to analyse the contribution and effect of each parameter independently.

Finally, it should be noted that both the simulations for different wind speeds and for different water current speeds change the equilibrium conditions of the global system, due to the existence of additional external forces. This issue will be analysed in the next section before replicating the analysis performed in Chapter 4.

5.2. Description of the analysis for the determination of modal properties

5.2.1. Determination of equilibrium points

Due to the issue mentioned in the end of the last section, whenever a new wind speed or water current was studied in the different degrees of freedom, it was necessary to previously carry out a simulation in which only the wind or water current were present, that is, without any displacement imposed on any of the degrees of freedom. From these simulations, it is possible to obtain the new equilibrium point of the system for that given wind speed or water current.

Considering and including these values of the new equilibrium points is essential so that the same simulation conditions can be guaranteed, thus allowing the results of both the reference values and the rest to be compared.

The scheme presented in Figure 5.1 exemplifies a little better this factor being taken into account for the surge motion.

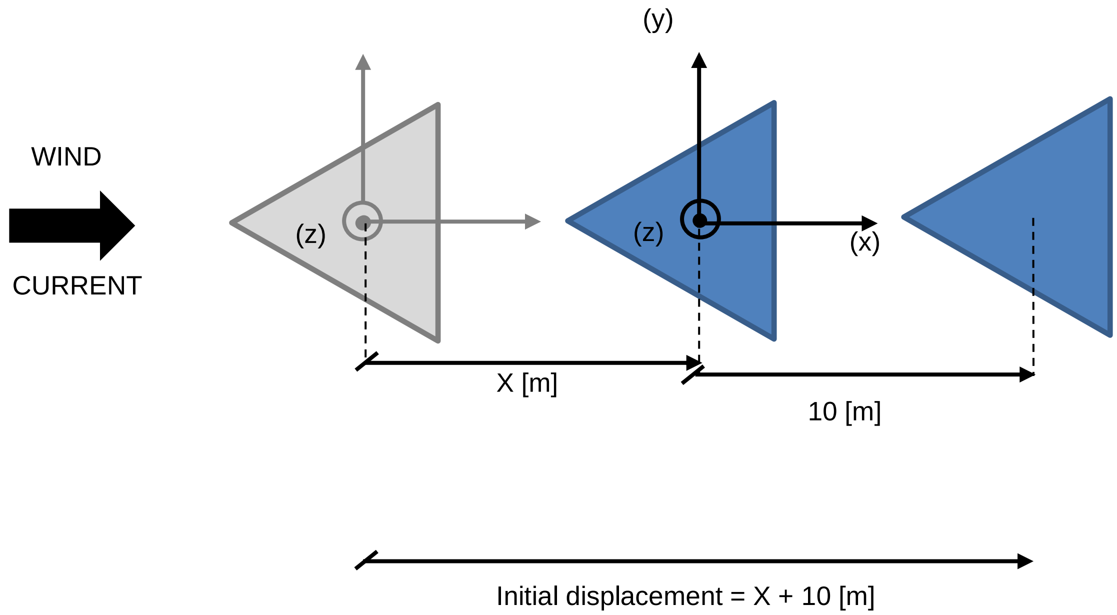

Figure 5.1 – Equilibrium point and initial displacement for surge analysis

The triangles symbolize the floating platform as seen from above, and in this case, it was illustrated how to arrive at the total displacement that must be inserted in the simulation to contemplate both the displacement due to the action alone (wind or water current) and the initial displacement tabulated for each degree of freedom (Table 4.1.).

The first triangle would be the reference for a situation without wind and without water current, the second is the platform already with the displacement due only to the action of the wind or water current (displacement represented by the unknown X, which varies according to each scenario). And finally, the third triangle already has both the displacement due to the action and the addition of the initial displacement that serves to study the behaviour of the turbine in each of the degrees of freedom (in this case 10m would be the initial displacement for the surge direction).

It is noteworthy that these equilibrium points were found for different scenarios and for all directions. These equilibrium values, that depend on the environmental conditions being considered, were always included in all the simulations and then, for the simulations of each specific degree of freedom, the predefined initial displacement of that direction was added. That is, when simulating the behaviour of the system, for example, in the surge direction, the value of the new equilibrium points of all directions were included (surge, sway, roll, pitch and yaw), but the final value of the initial displacement in the surge direction would be the value of the equilibrium point added to the predefined 10m. This process was repeated for all other degrees of freedom.

Table 5.2 below shows the different initial conditions for one of the different scenarios.

Table 5.2 – Initial displacements table format

Wind = 3 m/s (OFF)						
Platform direction	Surge [m]	Sway [m]	Heave [m]	Roll [º]	Pitch [º]	Yaw [º]
New equilibrium point	0.093	0.000	-0.009	0.004	-0.054	-0.003
Increment to equilibrium point	10	10	2	5	5	10
Total initial displacement	10.093	10.000	1.991	5.004	4.946	9.997

This analysis is also made for all other wind and water current scenarios. In Table 5.3 are compiled the values for each direction for all wind scenarios.

Table 5.3 – Equilibrium points summary (wind speeds)

	Equilibrium points					
Wind Speeds [m/s]	Surge [m]	Sway [m]	Heave [m]	Roll [º]	Pitch [º]	Yaw [º]
0 (blade pitch 20 º)	0.000	0.000	0.000	0.000	0.000	0.000
3 (blade pitch 20 º)	0.093	0.000	- 0.009	0.004	-0.054	-0.003
8 (blade pitch 0 º)	6.604	0.039	0.270	0.219	2.646	0.014
11.4 (blade pitch 0 º)	10.581	0.186	0.801	0.394	4.722	0.119
22 (blade pitch 20 º)	5.639	- 0.041	0.170	0.280	1.938	- 0.807
30 (blade pitch 20 º)	7.906	0.025	0.343	0.393	2.751	- 0.305
30 (blade pitch 90 º)	3.377	0.019	0.052	- 0.066	0.736	0.059

From table 5.3 it can be noted that in general as the wind speed increases so do the displacements of the equilibrium points. Something intuitive, but care must be taken, since for different wind speeds there are different blade pitch angles.

The effect produced by different blade pitch angles is more understandable when this parameter is isolated, for example in the last two lines of the table where for the same wind speed there are two different blade pitch angles. And as expected, the lower the blade pitch angle, the greater the impact of the wind on the wind turbine. This is because for parked conditions the smaller the blade pitch angle, the greater the thrust force acting on the rotor. The same can be verified for the operating conditions, in which even for a stronger wind, due to a higher blade pitch, the displacements are not greater. This shows that the blade pitch has a greater impact on the change in the equilibrium point than the wind speed.

In Table 5.4 are compiled the values for each direction for all water current scenarios.

Table 5.4 – Equilibrium points summary (water current speeds)

Water current speeds [m/s]	Surge [m]	Sway [m]	Heave [m]	Roll [º]	Pitch [º]	Yaw [º]
0	0.000	0.000	0.000	0.000	0.000	0.000
0.25	0.320	0.000	- 0.010	0.000	- 0.096	0.000
0.5	1.269	0.000	- 0.012	0.000	- 0.138	0.000
0.75	2.779	0.000	- 0.020	0.000	- 0.207	0.000
1	4.747	0.000	- 0.037	0.000	- 0.299	0.000

In this case, as the only parameter that changed are the water currents, as they increase, the displacements of the equilibrium point also increase.

Something that could be observed in both cases, the degrees of freedom that most suffer alterations in the equilibrium points are precisely the directions that the wind and water current directly affect. That is, surge and pitch. Note that the units are different, surge is in meters and pitch is in degrees. This effect can be more clearly seen in Figure 5.2 and Figure 5.3 that shows the different equilibrium point in surge and pitch directions for different wind speeds, and in surge direction for different water current speeds, since it was the only direction that suffer most impacts.

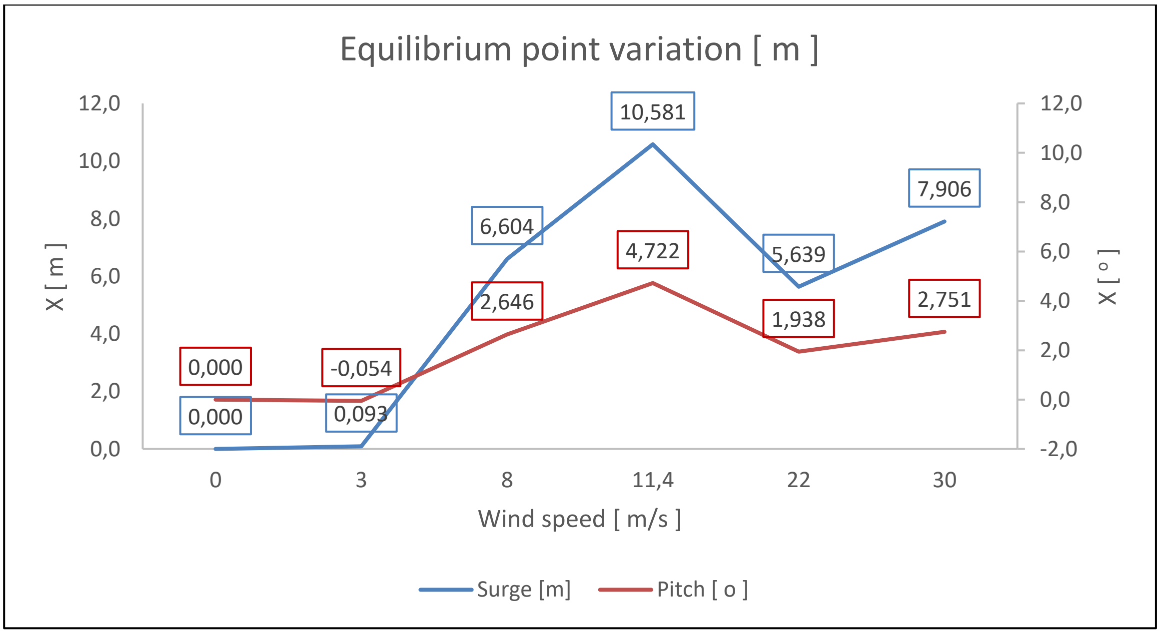

Figure 5.2 – Equilibrium points most affected by wind

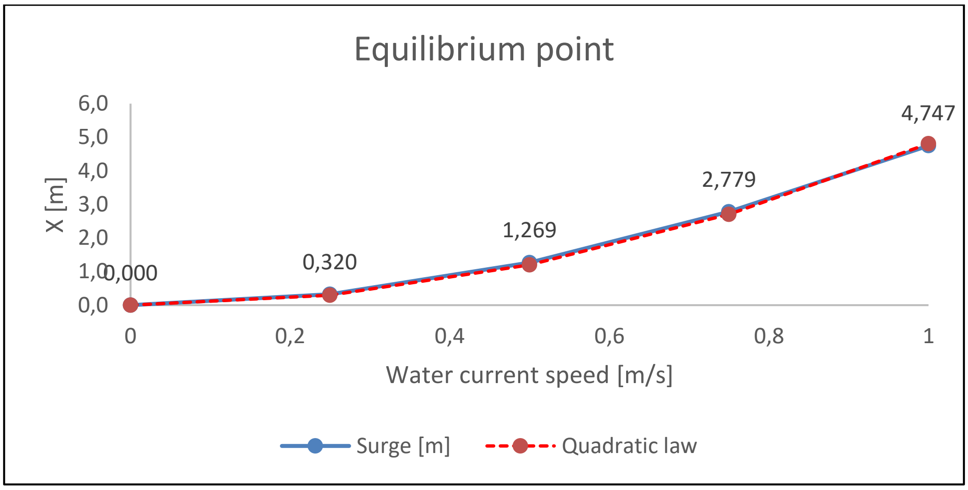

Figure 5.3 – Equilibrium points most affected by water current: surge direction

In Figure 5.3 is possible to note that the values of the equilibrium point increase in a quadratic relationship with the increase in current velocity because the hydrodynamic forces are proportional to the square of the velocity. The dashed red line was obtained following equation 5.1 for an example.

$$y = 4.80 \cdot x^2 \tag{5.1}$$

5.2.2. Tuning of the analysis parameters

Before presenting all the results for the different scenarios presented above, during the post-processing stage of the data obtained and their interpretation, some barriers encountered had to be overcome. These difficulties will now be mentioned as well as the decisions taken to overcome them.

First of all, once noticing that the results for each simulation (each degree of freedom) could have been mostly linked with either linear and/or nonlinear contributions models, for those which had practically only linear contributions the graph that once shown a linear trendline to explain the damping ratios distribution by the motion amplitude, with the corresponding values for $\boldsymbol{\xi_2}$, $\boldsymbol{\xi_1}$ and $\boldsymbol{\xi_0}$, now would be more adequately characterised by the mean value and standard deviation. This is equivalent to defining $\boldsymbol{\xi_0}$ and setting $\mathbf{m_\xi = 0}$.

Below, a case is shown in which the response of the structure can be practically represented by a linear damping model, which means that the distribution of the representation of the damping ratios by the motion amplitude is around an average value with a given dispersion.

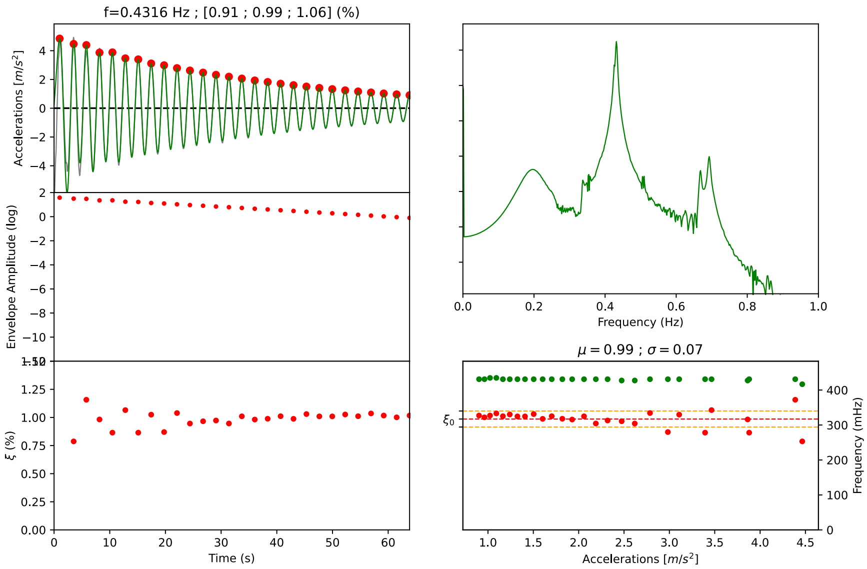

Figure 5.4 – Response of a simulation in FA direction for the reference value

Another obstacle found is that for simulations in which the damping ratios are very high there are few points to characterize the response well. In these cases, to estimate the value of **ξ_1**, which before was the corresponding value for an amplitude equal to 5% of the initial one, an amplitude equal to 1% of the initial one was used. All cases in which this criterion was adapted will be appropriately flagged. These situations occurred mainly in the water current simulations, as for instance in the case represented in Figure 5.5.

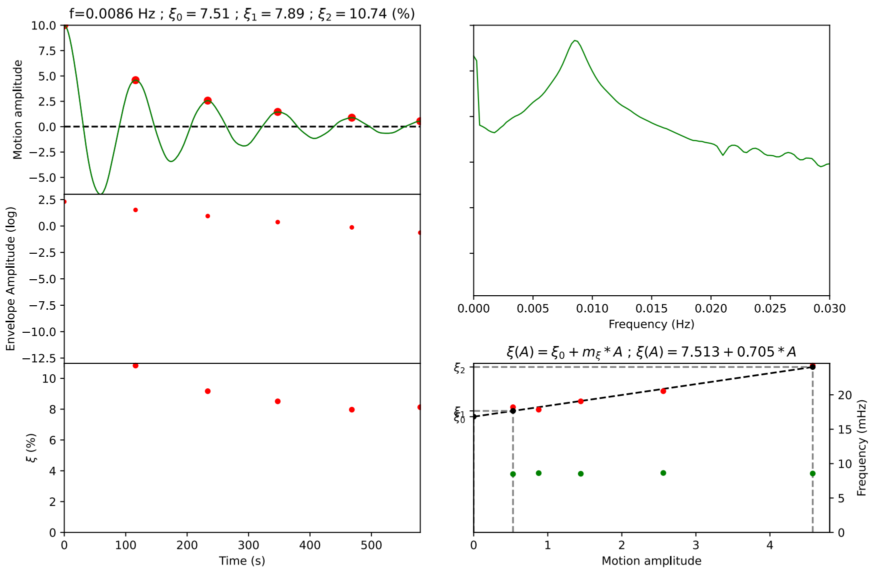

Figure 5.5 – Response of a simulation in sway for a current of 0.50 m/s

Another stumbling block encountered during post processing is that all results for simulations of the tower's degrees of freedom, FA and SS directions, are very polluted by other modes and therefore their analysis implied the application of filters. In addition, as the damping of the tower in general is much smaller than that of the floating platform, there are many more points until reaching 5% of the initial amplitude, which was the criterion adopted to find the value of ξ_1. Because of this, only the points up to 10% of the initial amplitude were used, to disregard numerical errors and ensure that only the mode being studied is being analysed. Again, these situations will be duly flagged.

Table 5.5 shows all the simulations that were carried out and indicates the appropriate cases in which there were changes in criteria for a better interpretation and reading of the results.

Table 5.5 – Criteria adopted for each simulation

	Reference	W = 3 m/s	W = 8 m/s	W = 11.4 m/s	W = 22 m/s	W = 30 m/s	W = 30 m/s	C = 0.25 m/s	C = 0.50 m/s	C = 0.75 m/s	C = 1.00 m/s
Surge								|	+	+	+
Sway								|	+	+	+
Heave											
Roll							—				
Pitch			—	—	—	—					
Yaw									—	—	—
FA	+	+		|	+	|	+	+	+	+	+
SS	+	+		+	+	+	+	+	+	+	+

Legend

No filter			Trend line			Percentage of A1 to obtain ξ_1	1%	5%	10%
With filter	|		Mean	—					

An interesting point to highlight is that for practically all simulations, for the FA direction of the tower, in which the wind turbine is not in operation (except for the wind of 11.4 m/s and 30 m/s with blade pitch of 20º), the averages were analyzed, which means that the model that best describes the behavior of the tower in this direction is mostly explained by a linear model. When looking at the SS, for all scenarios the averages were also analyzed.

Now that all the particularities of the simulations have been discussed, it is possible to move on to the analysis and interpretation of the results.

5.3. Impact of wind conditions

5.3.1. Platform

Starting by analysing the platform frequencies, something that immediately stands out is that in some directions there is practically no change in the frequency value regardless of the wind speed. In others there is quite a difference, that should be properly explained. This effect is particularly relevant in the surge and sway directions, as can be seen in Figure 5.6.

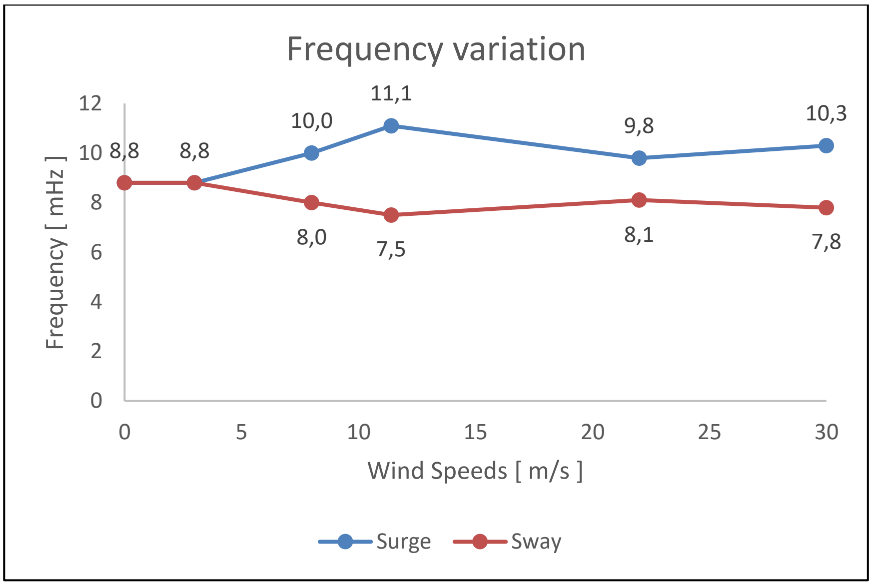

Figure 5.6 – Frequency variation in surge and sway DOFs

If only the variation for surge is analysed, the frequency gradually increases with increasing wind speed, up to 11.4 m/s and suddenly decreases for a higher wind (22 m/s) and then increase again. Note that the sway behaves the same, but symmetrically and at different intensities.

If the values of the equilibrium points are resumed (Figure 5.2), a behavior very similar to what is observed in the frequencies can be seen.

The main change in structural terms that the different equilibrium points cause is precisely the configuration of the mooring cables arrangement. Which in turn change the stiffness of the system, as some cables are more tensioned, and others are looser, changing the effective stiffness of the system, and hence its natural frequencies.

In summary, for different conditions of wind, the greater the displacement of the equilibrium point on the axis of the incident external action, the greater the stiffness in this direction and, consequently, the greater the frequency in the surge direction. However, the greater the stiffness in the action axis, the smaller the stiffness in the perpendicular axis, which causes the frequency in the sway direction to decrease with the increase in the translation of the equilibrium point.

Since the roll and pitch movements occur on the same axes as surge and sway, these movements also have the same behaviour, as can be seen in Figure 5.7

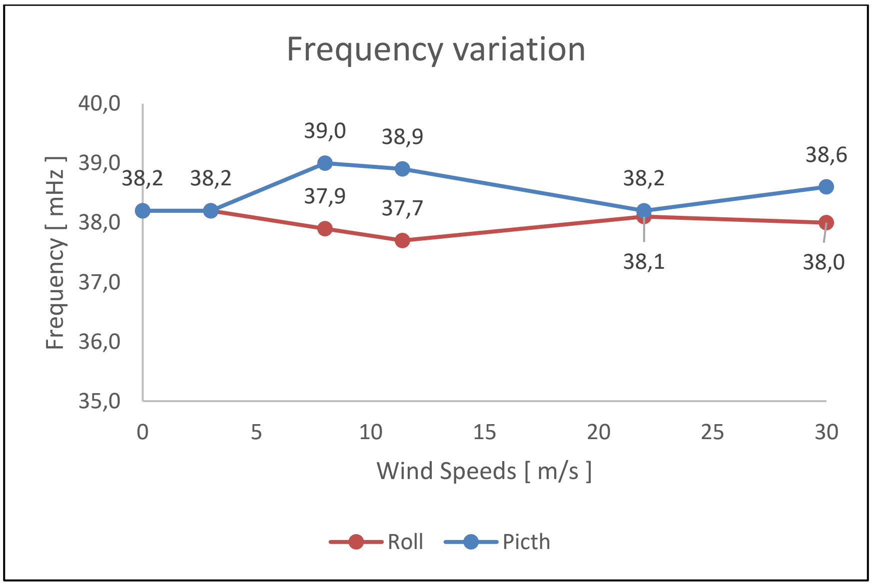

Figure 5.7 – Frequency variation in roll and pitch DOFs

Since yaw rotation is a movement with relative displacements on the same axes as surge and sway, a similar variation is also noted. As can be seen in figure 5.8.

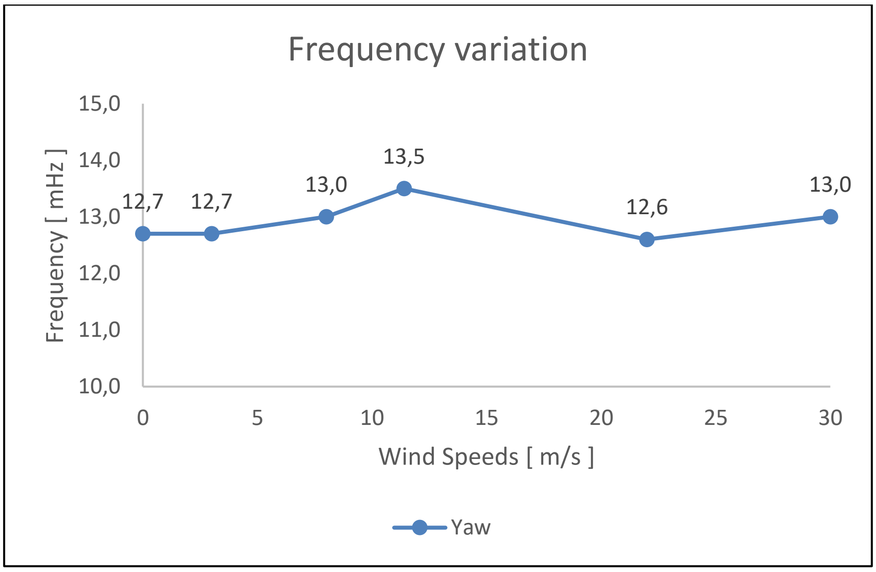

Figure 5.8 – Frequency variation in yaw DOF

For the last direction, heave, the frequencies remain much more stable, as can be seen in Figure 5.9.

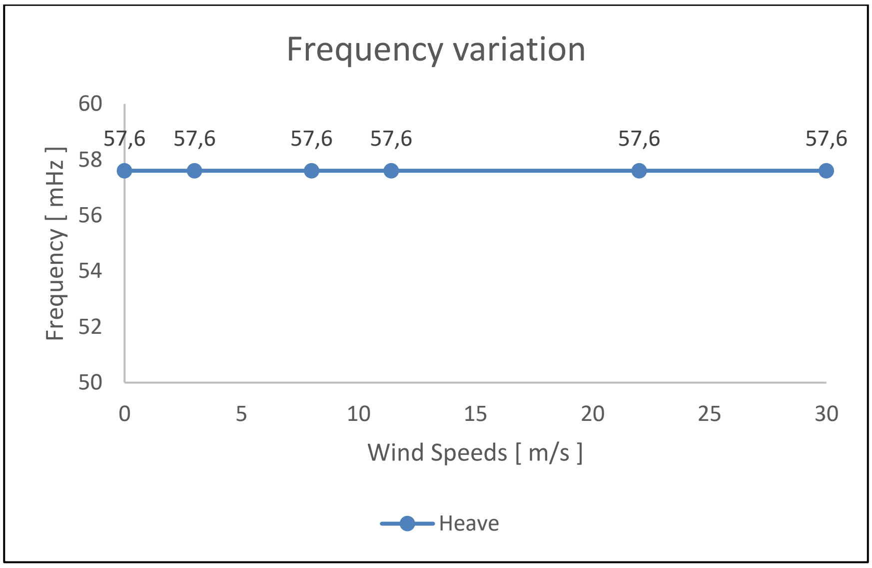

Figure 5.9 – Frequency variation in heave DOF

In figure 5.10, three graphs are presented to show the correlation of the frequency variation as a function of the displacement of the equilibrium point in the surge direction.

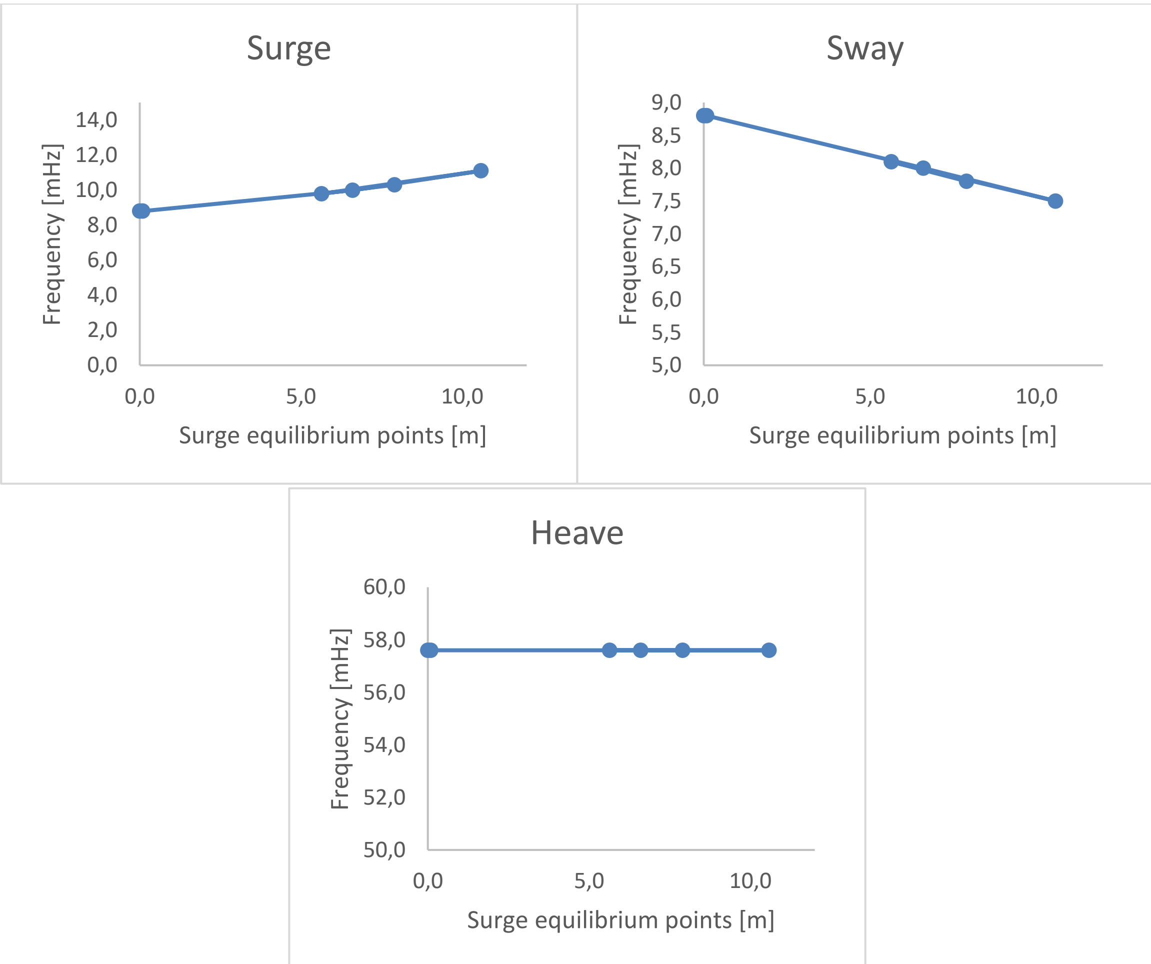

Figure 5.10 – Frequency variation as function of the displacements of the equilibrium point

Finally, if the scenarios in which only the blade pitch is changed are compared, as can be seen in Table 5.7, it is possible to notice, as expected, that the greatest impact is once again on the balance point, which ends up changing the frequencies, affecting the degrees of freedom in the same way as before (surge and pitch increasing and sway and roll decreasing).

Table 5.7 – Frequencies for different blade pitch angles

Blade Pitch	20º	90º	
F [mHz]	W = 30 m/s	W = 30 m/s	Increase or decrease
Surge	10.3	9.3	-10%
Sway	7.8	8.4	+8%
Heave	57.6	57.6	-
Roll	38.0	38.4	+1%
Pitch	38.6	38.2	-1%
Yaw	13.0	12.6	-3%

Moving now to the values found for $\boldsymbol{\xi_0}$, the degrees of freedom that had the greatest variation in values were, as expected, surge, pitch, and yaw, as represented in Figure 5.11. All three are associated with displacements that are on the axis of the imposed external action, so it was expected that they would be the ones that would suffer the most impacts. It is also notable that damping tends to be higher when the turbine is in operation, something that was expected.

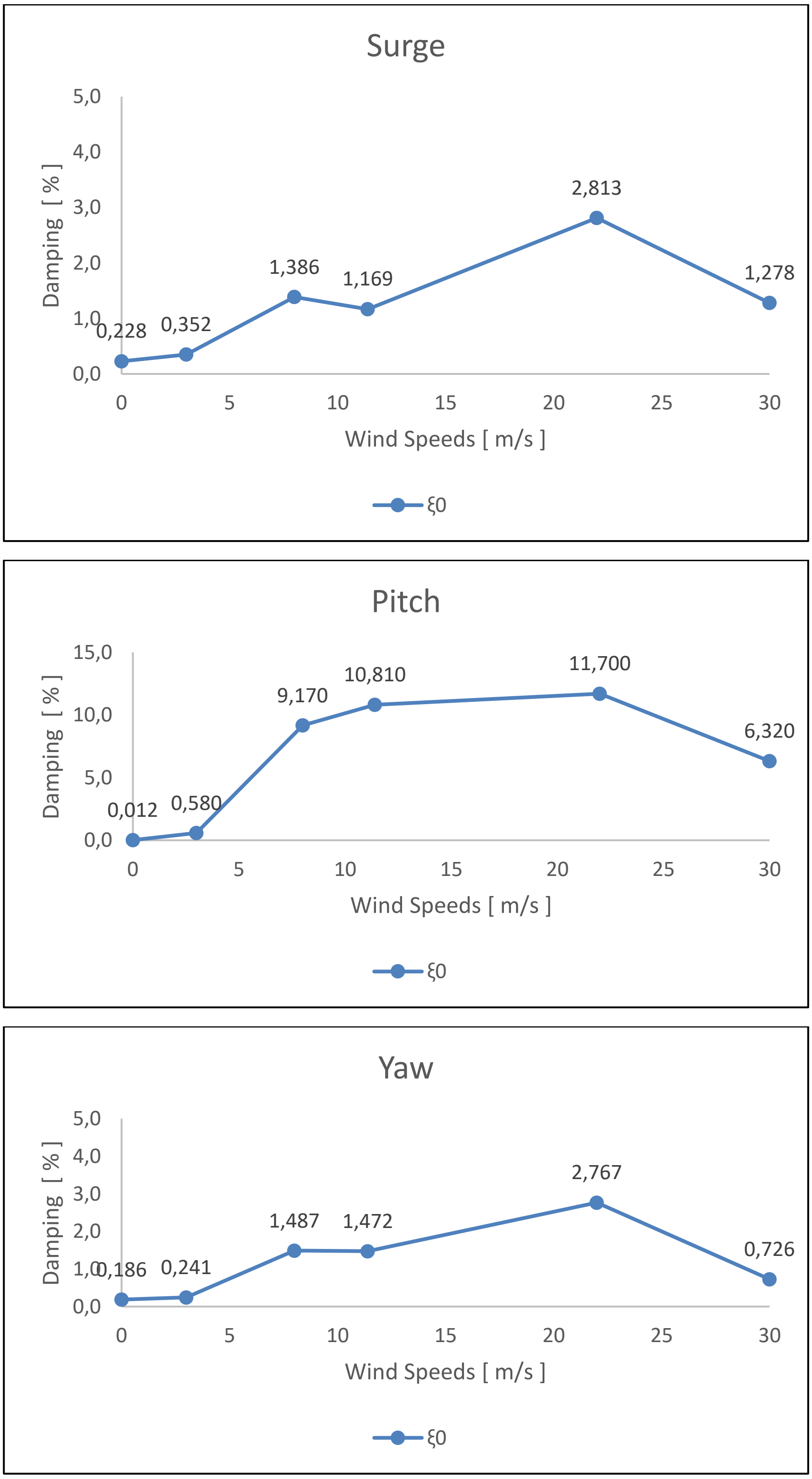

Figures 5.11 – Damping ratio ξ_0 for the most affected DOFs

All the other directions had a variation as well, but in a much smaller scale, as can be seen in Figure 5.12.

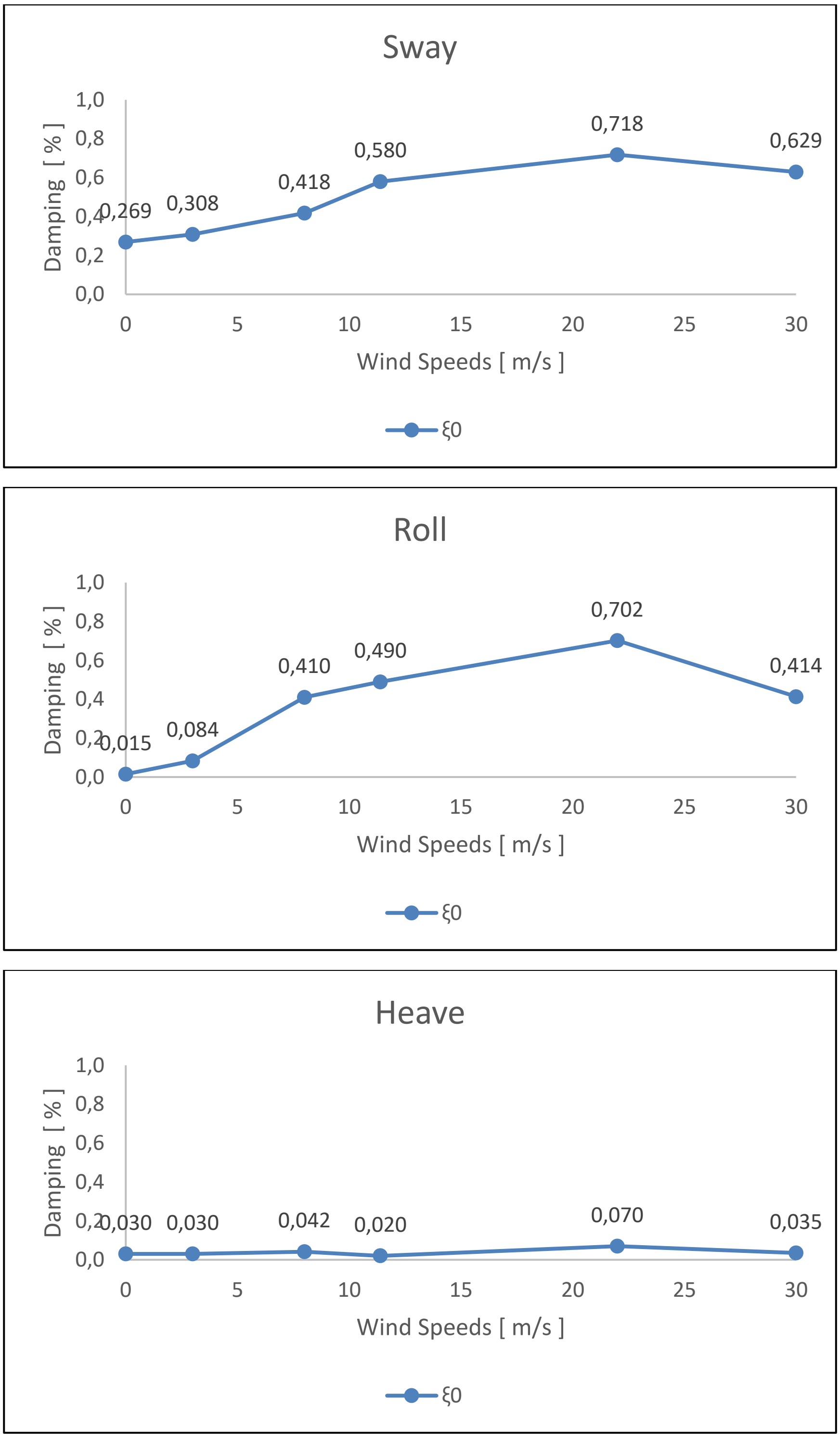

Figures 5.12 – Damping ratio ξ_0 for the least affected DOFs

Table 5.8 presents the damping values for the same wind of 30 m/s but with the blades pitch angle changing from 20º to 90º. With this, it is possible to perceive the greatest impact caused by the change of the blades angle.

For surge, pitch and yaw the damping value decreased, for the others it increased. With this it is possible to notice that the angle of the blades causes the damping in the degrees of freedom that are in the direction of the wind action, to decrease while in the perpendicular direction they increase. This is probably caused by the thrust action.

Table 5.8 – Blade pitch effect on damping ratio ξ_0

Blade Pitch	Pitch 20º	Pitch 90º	
ξ_0 [%]	W = 30 m/s	W = 30 m/s	Increase or decrease
Surge	1.278	0.695	-46%
Sway	0.629	1.516	141%
Heave	0.035	0.147	320%
Roll	0.414	6.830	1550%
Picth	6.320	1.135	-82%
Yaw	0.726	0.213	-71%

When analysing the $\mathbf{m}_\xi$, what is most significant is whether the value is equal to or different from zero, because, as already explained, if the $\mathbf{m}_\xi$ is equal to zero, it means that the damping ratios almost do not suffer variations and are distributed along an average value. In these cases, the model that best describes the behaviour of the structure for that given degree of freedom is a linear model and the value assigned to ξ_0 is the average value.

It is worth remembering that, as explained in Chapter 3, the value of $\mathbf{m}_\xi$ is related to the contribution of the nonlinear damping component. The results obtained for the translation and rotation degrees of freedom are presented in Figure 5.13 and Figure 5.14, respectively.

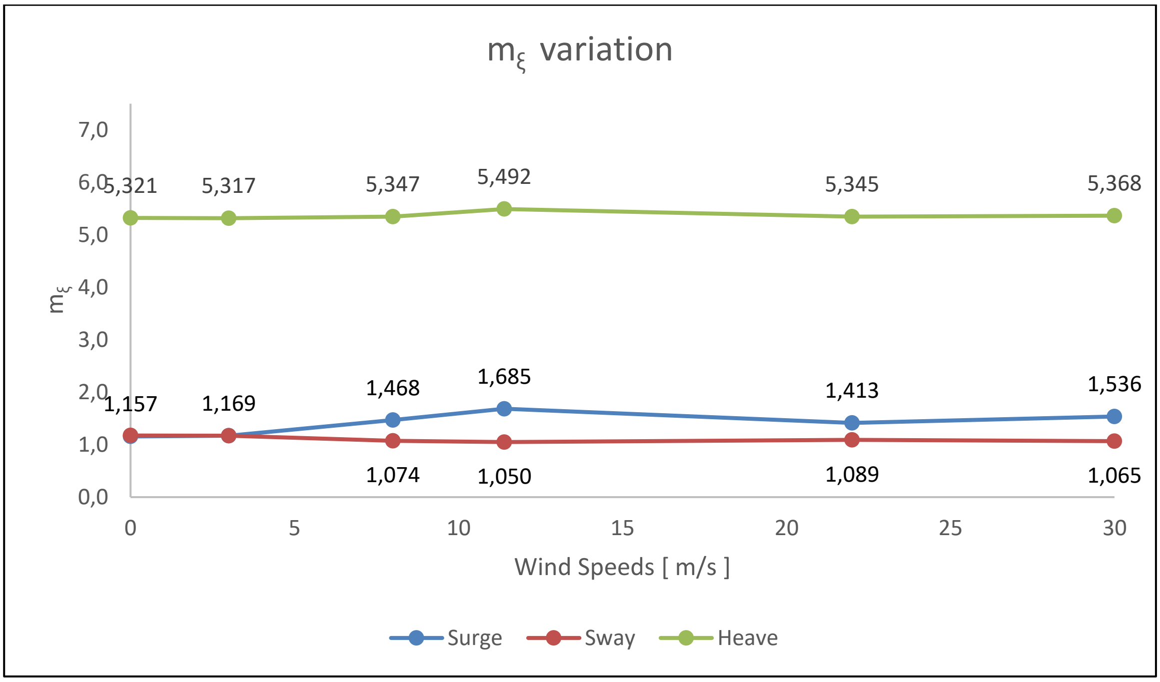

Figure 5.13 - $\mathbf{m}_\xi$ variation for translation DOFs

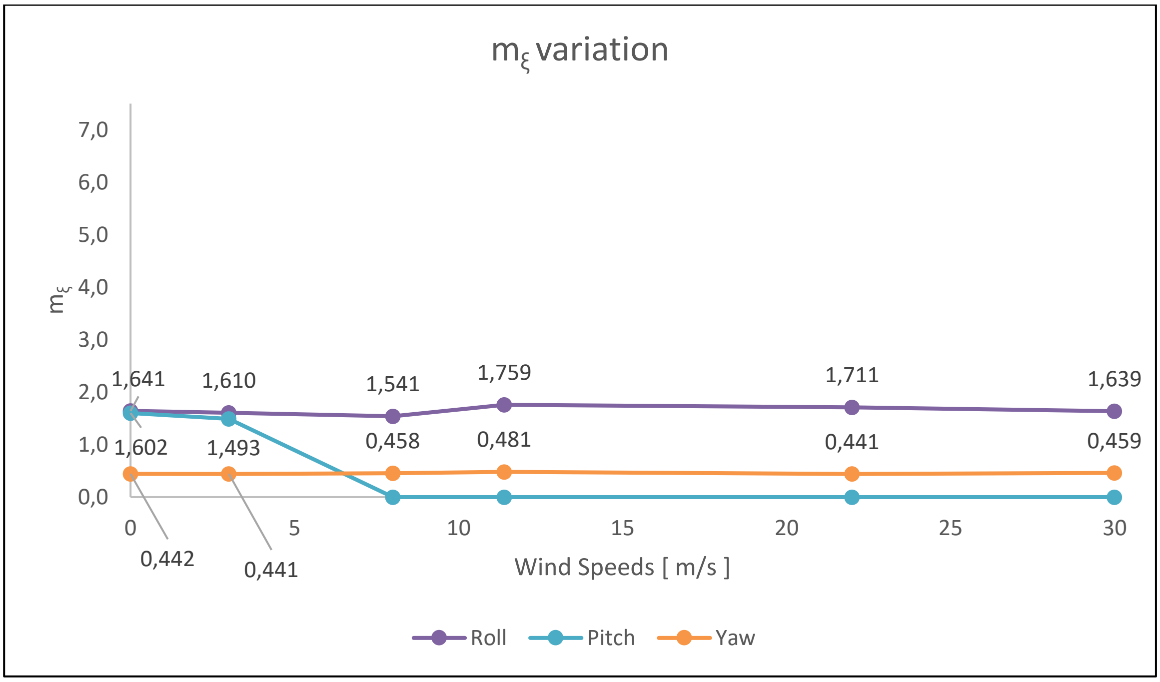

Figure 5.14 - $\mathbf{m}_\xi$ variation for rotation DOFs

As it is easy to see, the values suffer small variation, along the different wind speeds, and the cases in which the $\mathbf{m}_\xi$ is equal to zero is only for the pitch direction in the winds of 8 m/s, 11.4 m/s, 22 m/s and 30 m/s. It is worth noting that the value of $\mathbf{m}_\xi$ does not indicate whether the nonlinear component is large or small, but rather indicate whether it is present or not.

5.3.2. Tower

Moving on to the tower frequencies, FA and SS directions, a very uniform behavior is observed, since for the various modeled conditions there is almost no frequency variation when compared to the reference value.

The modeling in which the greatest frequency variation is observed is for the wind of 11.4 m/s in which the turbine is operating. When a turbine is in operation, the rotor rotates with a given angular velocity, in the case of the simulations carried out this speed is fixed since the wind speed is also fixed.

The 1P frequency is the frequency with which one of the blades passes through the tower, that is, if the rotor is rotating at a fixed speed of 12.1 rpm it means that the 1P frequency of this blade is 12.1 (rpm) / 60 (seconds) = 0.20167 Hz. Taking into account that the rotor has 3 blades, the frequency with which any one of the blades passes through the tower is called 3P and is equal to the value of 1P * 3, which in this case will be equal to 0.605 Hz.

If the 3P frequency is equal to or very close to the natural frequency of the tower, the phenomenon called resonance occurs. Resonance describes the phenomenon of increased amplitude that occurs when the frequency of an applied periodic force is equal or close to a natural frequency of the system on which it acts. When an oscillating force is applied at a resonant frequency of a dynamic system, the system will oscillate at a higher amplitude than when the same force is applied at other, non-resonant frequencies (Halliday, Resnick & Walker 2005, p. 324.).

For example, in the case of a wind of 11.4 m/s the natural frequency of the tower is 0.4472 Hz while the 3P frequency corresponding to a rotor at 12.1 rpm is 0.605 Hz, so there is no important amplification.

However, in the case of a wind of 8 m/s, the natural frequency of the tower found is 0.4451 Hz while the 3P frequency corresponding to a rotor at 9.2 rpm is equal to 0.46 Hz, so in this case resonance would occur. Therefore, this operating condition is not realistic and to simulate the wind turbine in operation it would be necessary to use the software control modules that prevent the rotor from working, for this wind speed, at this rotation speed and adjust it to a speed above or below, guaranteeing that there is no resonance.

Figure 5.15 shows two examples where the 3P frequency is visible. One of them does not generate resonance in the system because it is far enough away from the natural frequency of the tower (left image), the other is practically coincident (right image). This effectively prevents the tower FA response from being isolated and analysed.

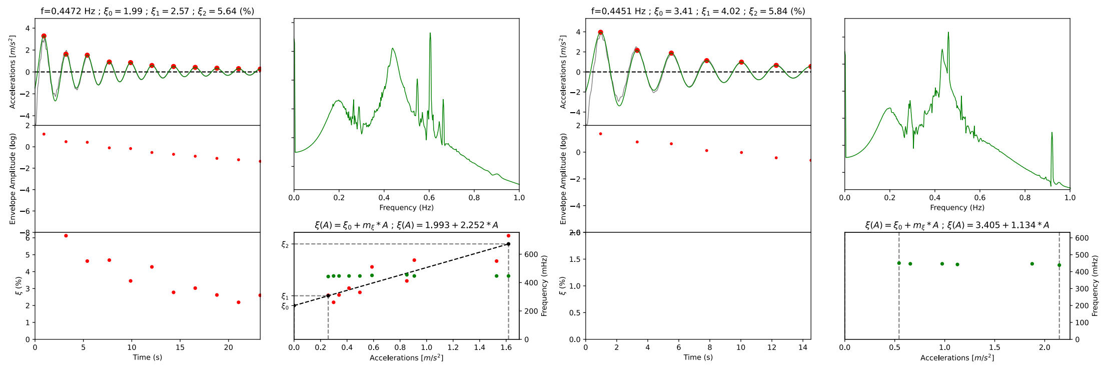

Figure 5.15 - Simulation to analyze the FA direction of the tower for a wind of 11.4 m/s to the left and a wind of 8 m/s to the right

The other results found for the tower frequencies, obtained from the accelerations, are shown in Figure 5.16.

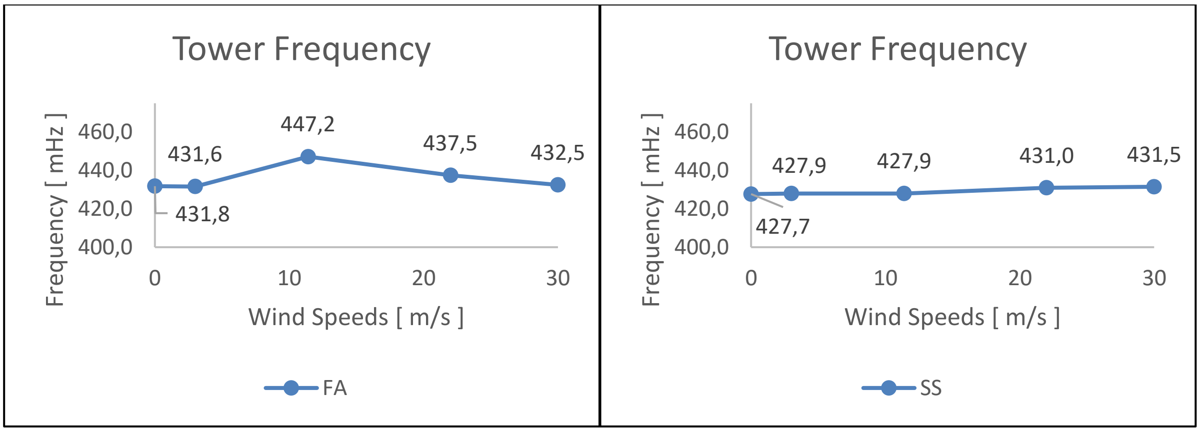

Figure 5.16 – Frequency variation for the main coupled modes of the tower

The effect that changing the blades pitch angle has can be compared in the table 5.9.

Table 5.9 - Blade pitch effect on tower frequencies (F)

Blade Pitch	20º	90º	
F [mHz]	W = 30 m/s	W = 30 m/s	Increase or decrease
FA	432.5	433.8	0%
SS	431.5	419.9	-3%

For the damping in both directions, the values are presented in figure 5.17, and it is possible to notice, as expected, the increasing of the damping ratio with the increase of the wind speed once the aerodynamic forces also increase.

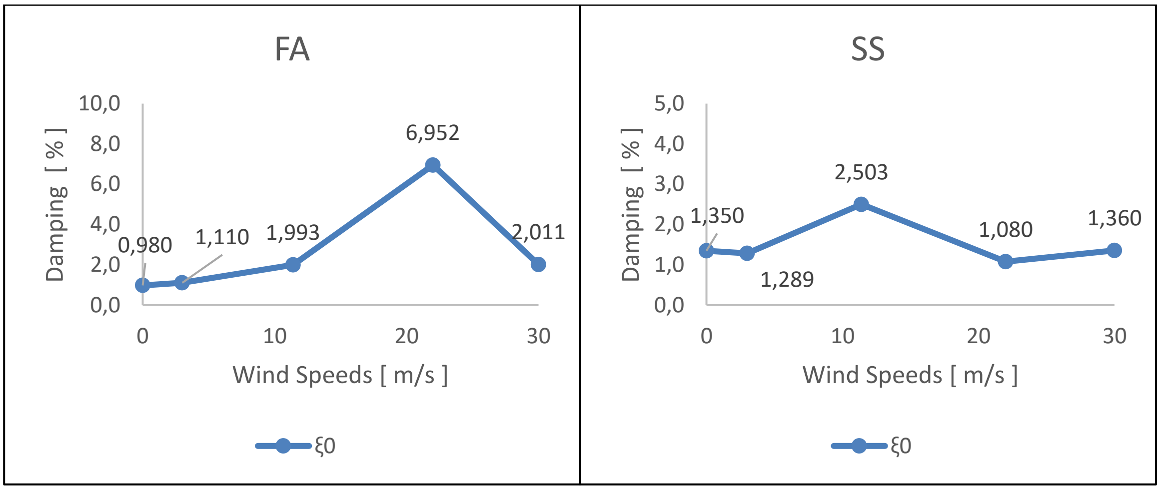

Figure 5.17 – Damping variation for the main coupled modes of the tower

For the same reason presented above, when the blades offer less resistance to the wind, facilitating the flow, the tendency is for the aerodynamic forces to decrease and consequently the damping in the direction of action (FA) also decreases, while increasing in the SS direction. The Table 5.10 and the Figure 5.18 shows these results.

Table 5.10 - Blade pitch effect on damping ratio ξ_0

Blade Pitch	Pitch 20º	Pitch 90º	
ξ_0 [%]	W = 30 m/s	W = 30 m/s	Increase or decrease
FA	2.011	0.850	-58%
SS	1.360	6.600	385%

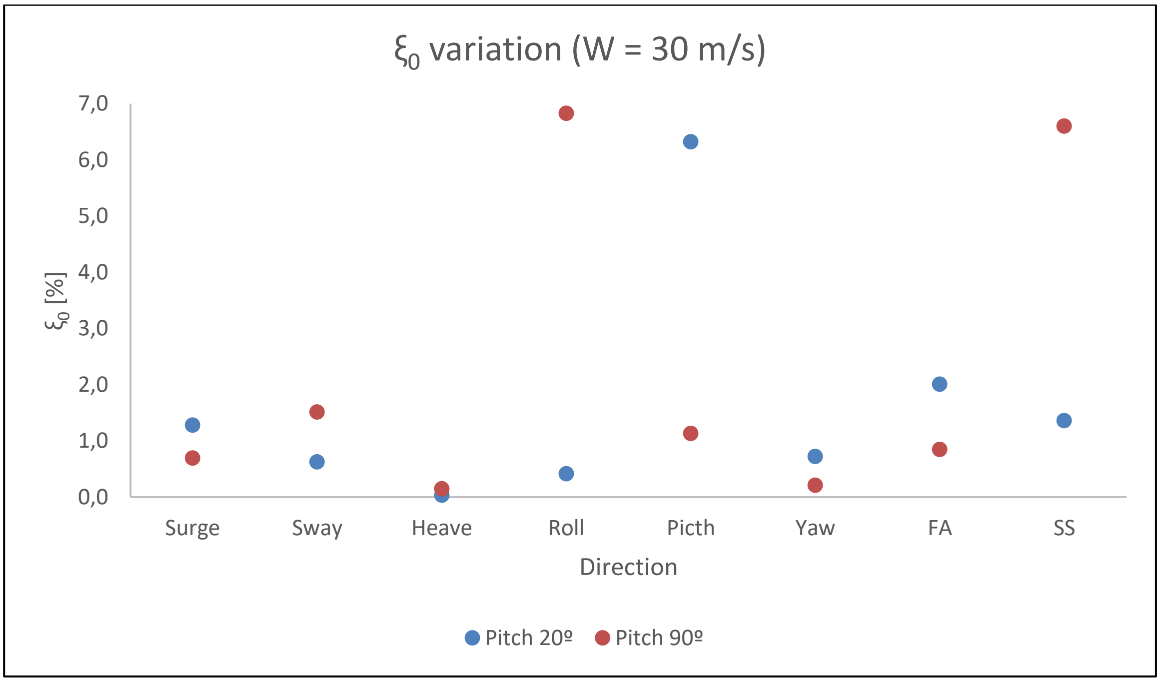

Figure 5.18 – Damping variation for different blade pitch angles

Moving on to the $\mathbf{m_{\xi}}$, the results are mostly due to contributions from the linear damping portion, so except for the winds of 11.4 m/s and 30 m/s in the FA direction, the averages were analyzed so $\mathbf{m_{\xi} = 0}$, as can be seen in Figure 5.19.

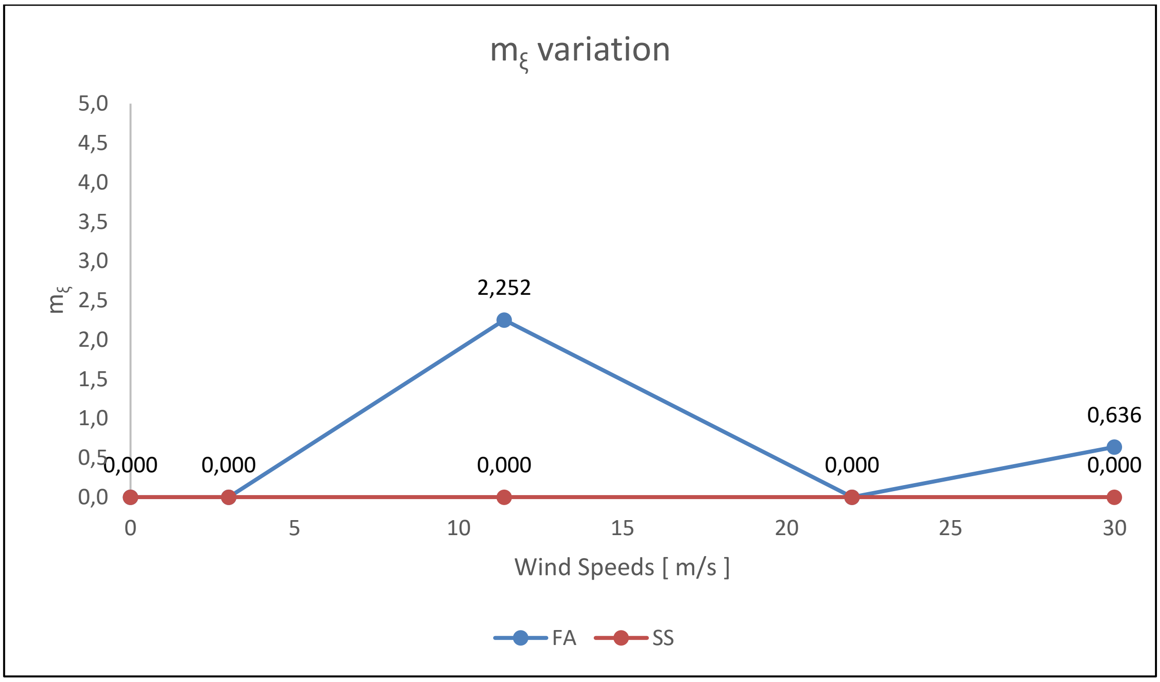

Figure 5.19 – Damping variation for the main coupled modes of the tower

5.4. Impact of current conditions

5.4.1. Platform

Starting the analyses with the frequencies, it is possible to observe that the responses for the current simulations are due practically to the same reason of the wind simulations, the change of the equilibrium point. With the increase in the translation of the equilibrium point, the higher the frequency in the surge direction and the lower the frequency in the sway direction. The difference is that now, as it can be seen in figure 5.3, the displacement of the equilibrium point is always increasing with increasing current.

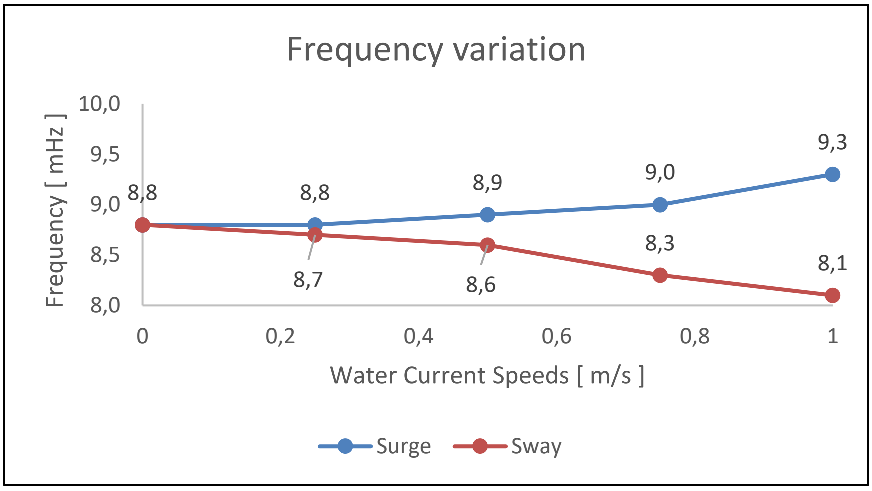

Figure 5.20 - Frequency variation in surge and sway DOFs

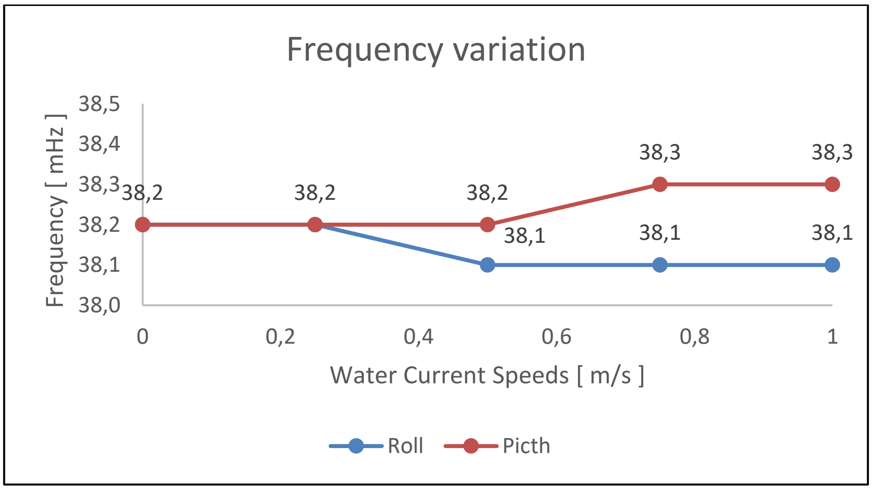

Figure 5.21 - Frequency variation in roll and pitch DOFs

Figure 5.21 shows a variation, albeit very subtle, and a behaviour similar to Figure 5.20. For movements in the z direction (heave and yaw), the frequency values remain practically the same for any current value.

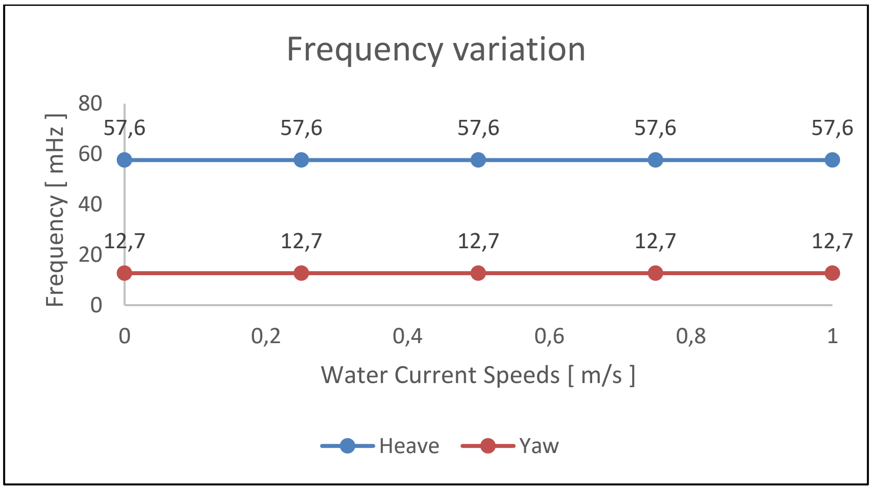

Figure 5.22 - Frequency variation in heave and yaw DOFs

Turning now to the damping ratios for the different water current velocities, it can be seen that the damping increases with the increase in current speed. But now, the directions that were most impacted were translation in x (surge) and rotation in z (yaw), which has relative displacements in the direction of the current. It was also possible to observe that the sway values are half of the surge values. The results are presented in Figure 5.23 and Figure 5.24.

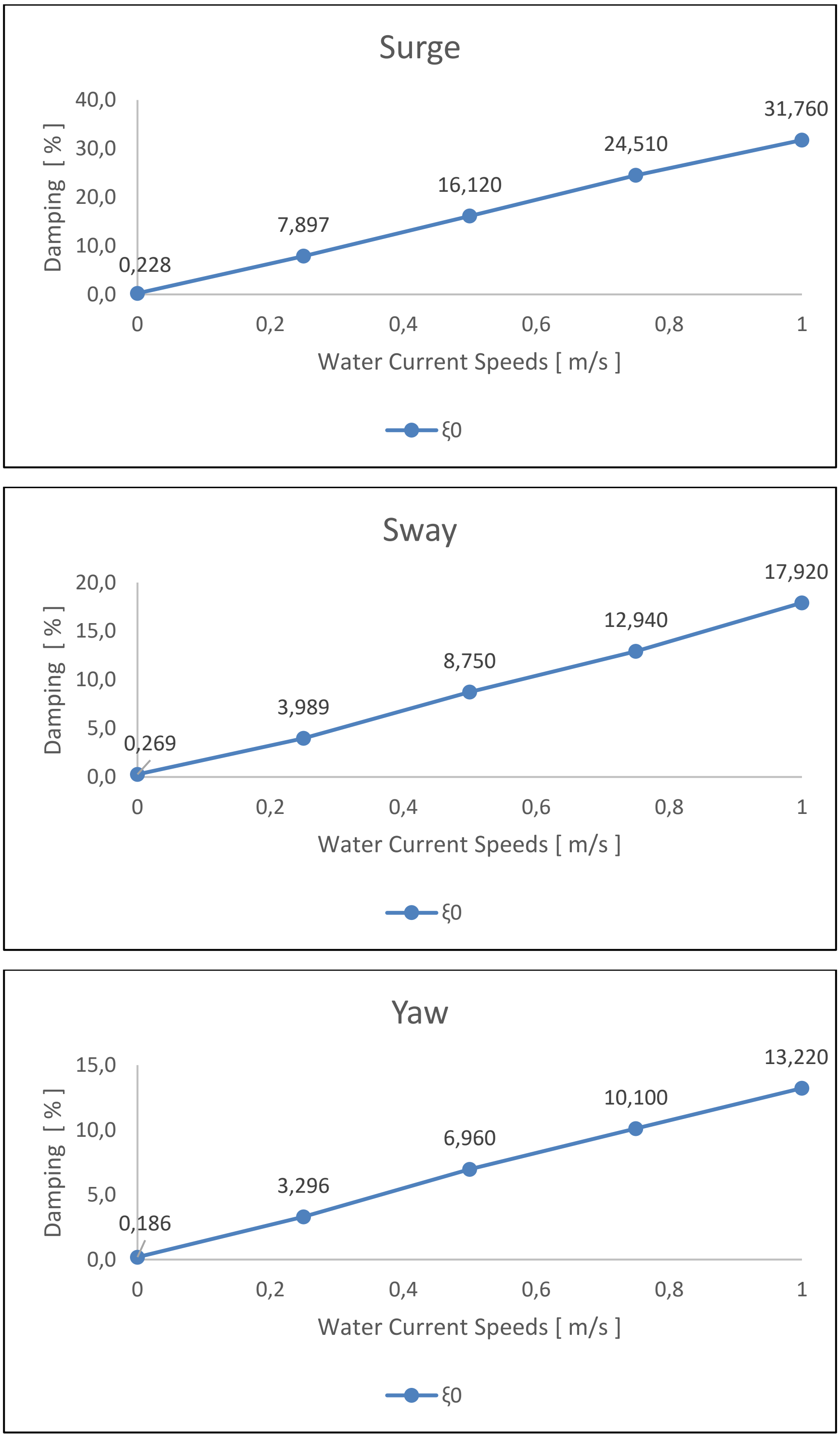

Figures 5.23 – Damping ratio ξ_0 for surge, sway and yaw

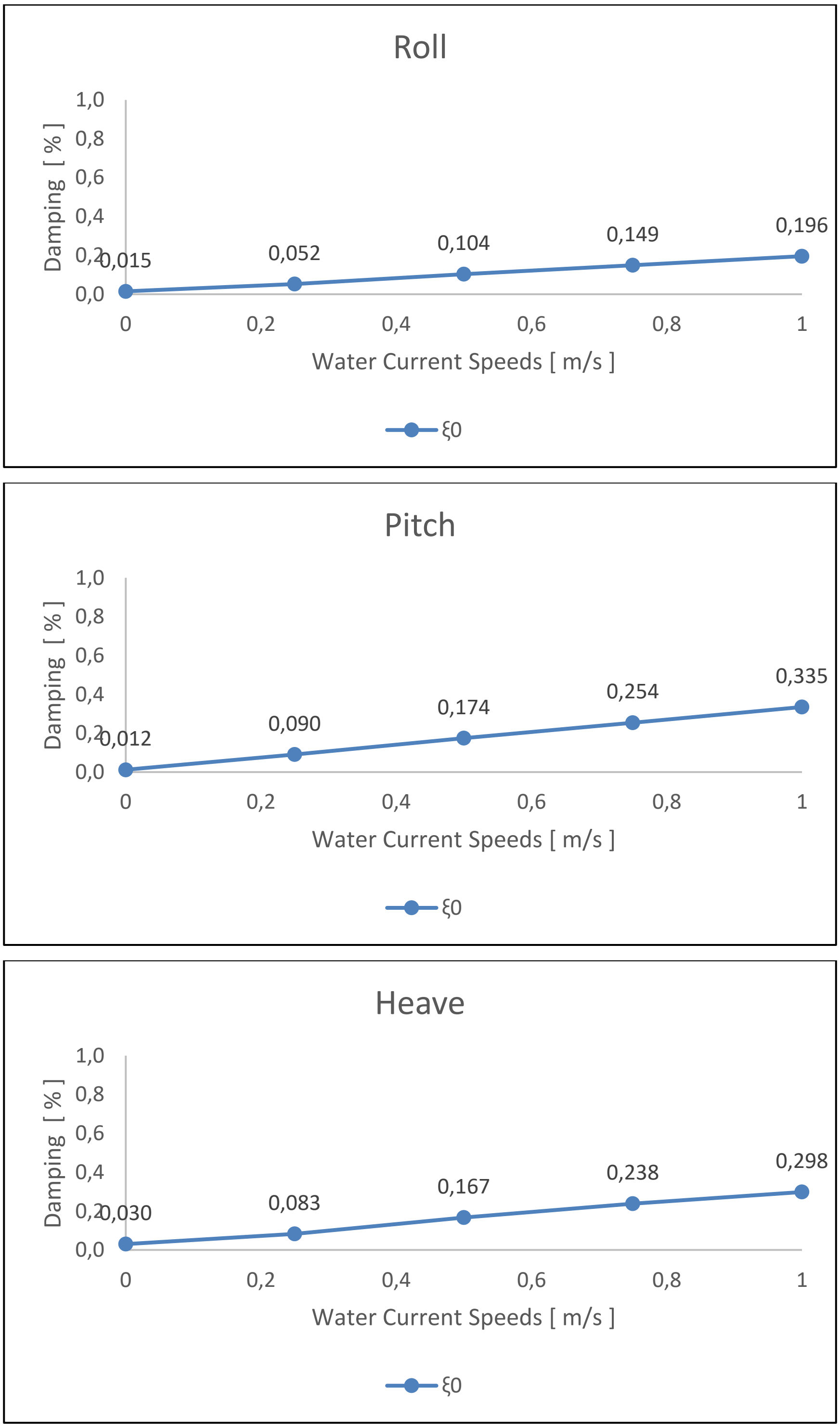

Figures 5.24 – Damping ratio ξ_0 for roll, pitch and heave

The ξ_0 analyzes for the platform, the surge and sway translations and the yaw rotation (which is a relative displacement in the current directions) were all, except for a current of 0.25 m/s, for mean values (**m_ξ = 0**) which indicates that in these directions the model that best describes the behavior is a model in which the contribution to damping is mostly from the linear portion.

For all other cases significant nonlinear contributions were verified. And the values are presented in Table 5.11 and Figures 5.25.

Table 5.11 - **m_ξ** variation for all DOFs

	Reference	Water Current Speeds (m/s)			
m_ξ	0	0.25	0.50	0.75	1.00
Surge	1.157	0.363	0.000	0.000	0.000
Sway	1.175	0.634	0.000	0.000	0.000
Heave	5.321	5.295	5.247	5.224	5.233
Roll	1.641	1.639	1.634	1.636	1.638
Pitch	1.602	1.595	1.597	1.602	1.606
Yaw	0.442	0.202	0.000	0.000	0.000

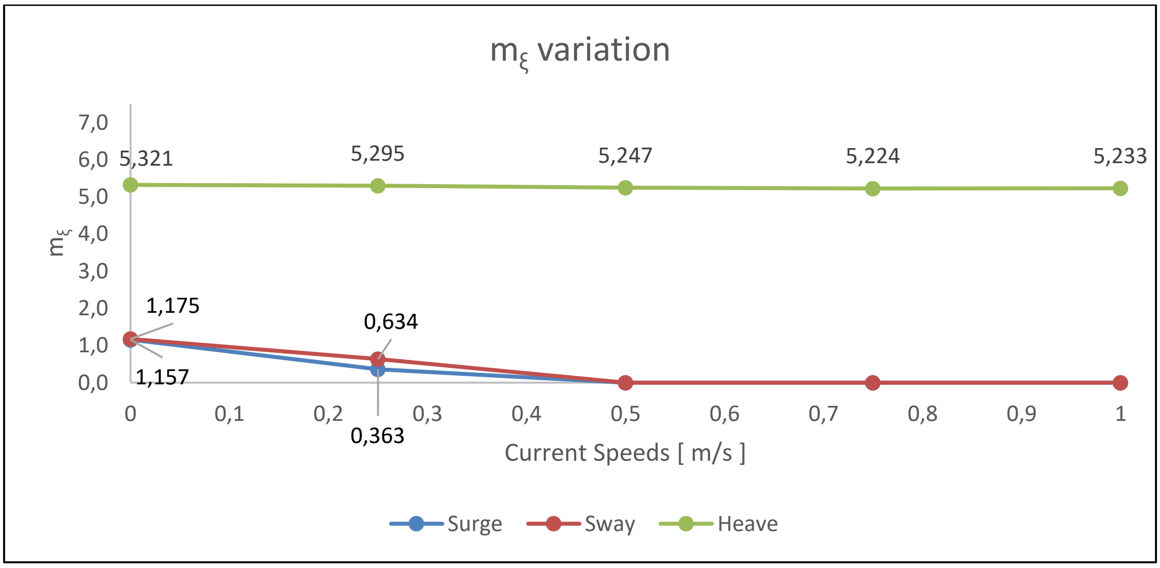

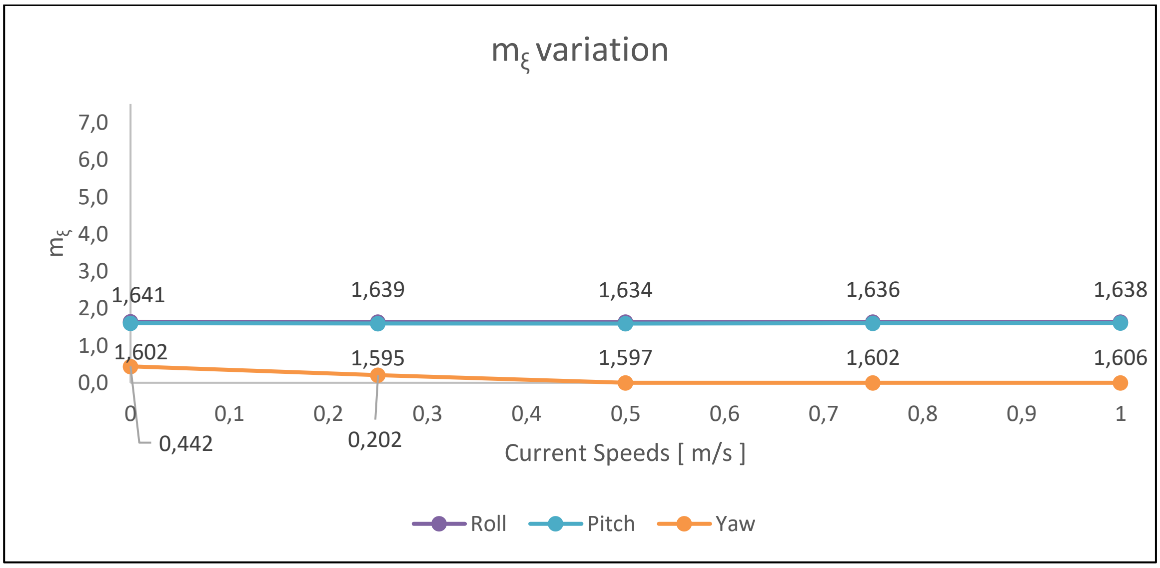

Figure 5.25 – **m_ξ** variation for different water current speeds

5.4.2. TOWER

The frequencies, obtained from the accelerations, for the main coupled modes of the tower, when compared with the reference values, practically did not change for the different currents.

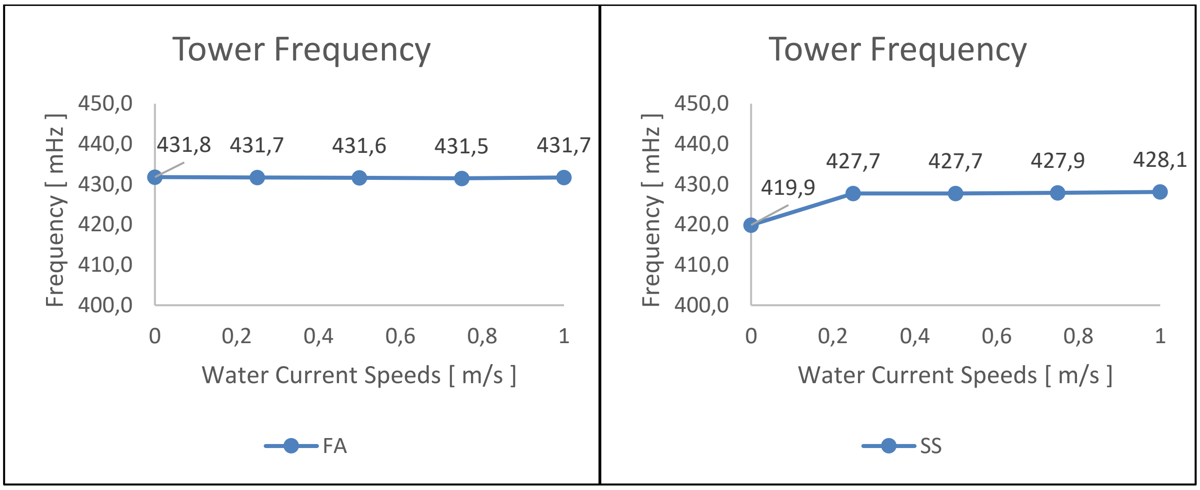

Figure 5.26 – Frequency variation for the main coupled modes of the tower

The values of the damping ratios $\boldsymbol{\xi_0}$ present small variations, being the one observed in the damping for the SS direction greater than for the FA direction.

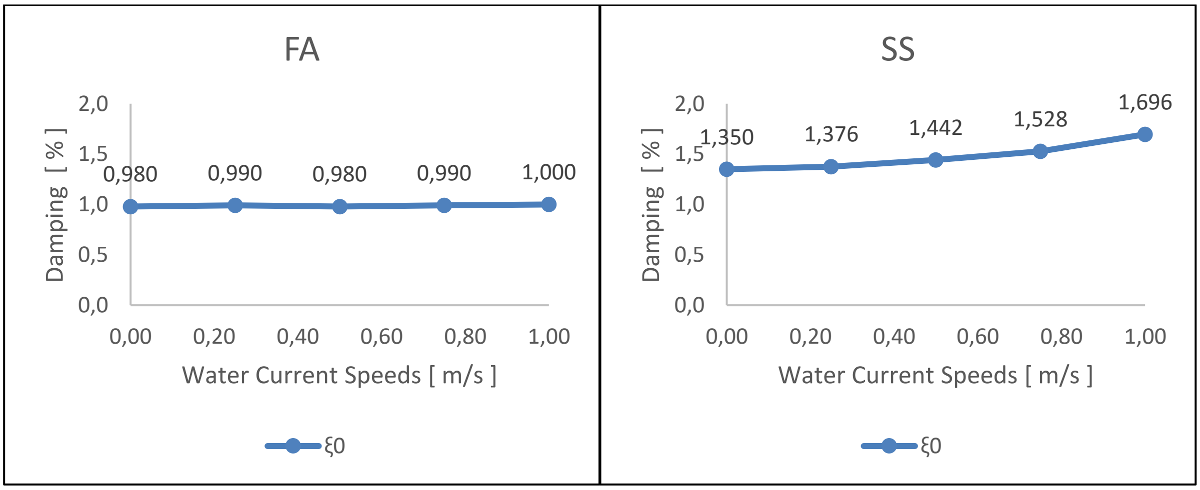

Figure 5.27 – Damping variation for the main coupled modes of the tower

Another point to highlight is that, for all current velocities, the means were analyzed for $\boldsymbol{\xi_0}$ ($\boldsymbol{m_\xi}$ is equal to zero), which means that for currents in general the model that best describes the behavior, for these conditions, are the models in which practically all the contribution to the tower damping comes from the linear portion.

5.5. FINAL REMARKS

Of all the results obtained and studied, some of the most relevant points should be highlighted.

One of the first factors discussed in this chapter was the influence that the displacement of the structure (change of equilibrium points), due to external actions, can have on the variation of frequencies, in some directions more than in others.

Regarding the damping ratios, for the wind, as expected, the directions that suffer the most relevant changes are those that coincide with the direction of the wind action (surge, pitch and yaw). This variation is not directly proportional to wind speed, since for different wind speeds there are different operating conditions (blade pitch angles and rotor speed) that end up also influencing damping.

When it comes to the current, there is a variation for damping directly dependent on the speed of the current, with an increase in current there is an increase in damping. However, this time the directions that are most impacted by the action are the translation (surge) and the yaw rotation, which in the end are the ones that present a relative movement aligned with the action of the current.

6
CONCLUSIONS

6.1. CONCLUSIONS

This work started with a familiarization with the components and working principles of floating wind turbines, discussed in Chapter 2.

This was followed by Chapter 3, in which there is a theoretical review of concepts that would be important during the course of the work, namely the ones associated with the dynamics of structures. In parallel with the learning and development in the area of programming, since it would be necessary for the management and analysis of the data then obtained from the simulations.

It was also necessary to study the software used in the simulations (OpenFAST) as well as the available simulation conditions and options.

Next, in Chapter 4, the type of simulations that would be performed and the parameters that would be studied were defined. It is worth noting that during the course of the work, several unforeseen issues had to be resolved and decisions had to be taken.

Finally, the simulations were performed, and the results obtained analysed in Chapter 5.

Some important conclusions with regards the system's natural frequencies could be draw from these results: it was observed a frequency dependence on the platform equilibrium point since these changes the stiffness of the system; it is also clear the symmetry and opposite behaviours between the surge and sway translation directions, as well as the roll and pitch rotations, both for wind and current scenarios.

Also, a correlation of the damping ratios with the motion amplitude could be observed. This correlation may be associated with the linear and/or nonlinear damping component, observed both for wind and current scenarios.

With the analysis of the influence of different blade pitch angles, it was noted the same symmetry and opposite behaviours between translations surge and sway, rotations roll and pitch and, this time, also for the tower FA and SS directions.

In summary, the results obtained in this thesis bring several important observations and open up many options to continue exploring both these results and to seek results for new simulations.

6.2. FUTURE WORK

One of the main follow-ups that can be done is to continue exploring the results found for the simulations carried out, which had the operating parameters and external conditions very controlled and try to verify if the results obtained can somehow constitute a base model for other different conditions of more realistic operation conditions. Wind and sea currents were analyzed separately; the analysis of combinations of both would be interesting.

In order to find the values of $\boldsymbol{\xi_0}$ and $\mathbf{m}_{\xi}$, controlled simulations were carried out with the imposition of an initial displacement, so it was possible to obtain the damping values for a given range of motion amplitudes. For the damping ratio estimation for a given scenario it is necessary to have as input the value of the amplitude (**A**) caused by specific external conditions, so that, together with the values of $\boldsymbol{\xi_0}$ and $\mathbf{m}_{\xi}$, it would be possible to obtain a value for the damping. The determination of these amplitudes for realistic operating condition on particular sites still needs to be done.

Another possibility, it is to perform operational modal analyses over numerical simulations of realistic operating conditions or using experimental data collected in operating floating wind turbines.

REFERENCES

Ahmad, I., M'zoughi, F., Aboutalebi, P. *et al.* A regressive machine-learning approach to the non-linear complex FAST model for hybrid floating offshore wind turbines with integrated oscillating water columns. *Sci Rep* **13**, 1499 (2023). https://doi.org/10.1038/s41598-023-28703-z

Balasubramanian, P. (2020). *Linear and Nonlinear Damping Identification in Vibrations of Thin-Walled Structures*. https://escholarship.mcgill.ca/concern/theses/b8515s59v

Cheever, Erik. "Introduction to the Fourier Transform," Department of Engineering at Swarthmore College. Accessed June 17, 2022.

Clough, R. W., & Penzien, J. (2003). *DYNAMICS OF STRUCTURES*. https://doi.org/10.1002/eqe.4290240311

Fourier, J. (1807). Mémoire sur la propagation de la chaleur dans les corps solides. Nouveau bulletin des sciences par la société philomathique de Paris, 1. 112–116.

Halliday D Resnick R Walker J. Fundamentals of Physics. 7th ed. Hoboken NJ: Wiley; 2005.

Hau, Erich. (2006). Wind Turbines: Fundamentals, Technologies, Application, Economics. 10.1007/3-540-29284-5.

James, R., and Ros, M. C. (2015). Floating Offshore Wind: Market and Technology Review. The Carbon Trust.

Jonkman, J. M. and Buhl Jr., M. L. FAST User's Guide, NREL/EL-500-38230 (previously NREL/EL-500-29798), Golden, CO: National Renewable Energy Laboratory, August 2005.

Jonkman, J.M. (2009), Dynamics of offshore floating wind turbines—model development and verification. Wind Energ., 12: 459-492. https://doi.org/10.1002/we.347

Kooijman, H. J. T., Lindenburg, C., Winkelaar, D., and van der Hooft, E. L., "DOWEC 6 MW Pre-Design: Aero-elastic modeling of the DOWEC 6 MW pre-design in PHATAS," DOWEC Dutch Offshore Wind Energy Converter 1997–2003 Public Reports [CD-ROM], DOWEC 10046_009, ECN-CX--01-135, Petten, the Netherlands: Energy Research Center of the Netherlands, September 2003.

Manolas, Dimitris & Riziotis, V. & Papadakis, George & Voutsinas, S.. (2020). Hydro-Servo-Aero-Elastic Analysis of Floating Offshore Wind Turbines. Fluids. 5. 200. 10.3390/fluids5040200.

Matha, Denis. (2009). Model Development and Loads Analysis of an Offshore Wind Turbine on a Tension Leg Platform with a Comparison to Other Floating Turbine Concepts: April 2009. 10.2172/973961.

Pacheco, J., & Magalhães, F. (2019). *INTRODUÇÃO AO FUNCIONAMENTO DOS GERADORES EÓLICOS E SUA MODELAÇÃO NUMÉRICA.*

Plodpradit, P.; Dinh, V.N.; Kim, K.-D. Coupled Analysis of Offshore Wind Turbine Jacket Structures with Pile-Soil-Structure Interaction Using FAST v8 and X-SEA. *Appl. Sci.* **2019**, *9*, 1633. https://doi.org/10.3390/app9081633

Ploetz, Reinhard and Rusdianasari, Rusdianasari and Eviliana, Eviliana (2016) *RENEWABLE ENERGY: ADVANTAGES AND DISADVANTAGES.* Proceeding Forum in Research, Science, and Technology (FIRST) 2016. ISSN 2461-0739

Savenije, Feike & Peeringa, Johan. (2014). Control development for floating wind. Journal of Physics: Conference Series. 524. 012090. 10.1088/1742-6596/524/1/012090.

SCADA — Generic Wind Farm Supervisory Control and Data Aquisition System, Sytem Specification, Garrad Hassan and Partners Ltd., Nov. 2001

Tartibu, Lagouge & Kilfoil, Maria & van der Merwe, A. (2015). Vibration Analysis of a Variable Length Blade Wind Turbine. International Journal of advances in Engineering and Technology. 4. 630-639. 10.7323/ijaet/v4_iss1.

Wagner, H.-J. (2013). Introduction to wind energy systems. EPJ Web of Conferences, 54, 01011

Welch, Peter D. The Use of the Fast Fourier Transform for the Estimation of Power Spectra: A Method Based on Time Averaging Over Short, Modified Periodograms. *IEEE Transactions on Audio and Electroacoustics* 15, no. 2 (1967): 70–73. ieeexplore.ieee.org/document/1161901.

File:Airfoil lift and drag.svg. (2023, February 25). *Wikimedia Commons*. Retrieved 19:30, June 9, 2023 from https://commons.wikimedia.org/w/index.php?title=File:Airfoil_lift_and_drag.svg&oldid=735770915.

https://acteon.com/blog/floating-wind-mooring-options/ accessed in 27/4/2023.

https://windeurope.org/about-wind/wind-energy-today/ accessed in 8-3-2023.

https://www.energy.gov/eere/wind/how-wind-turbine-works-text-version / accessed in 22-3-2023.

https://www.modec.com/business/newbiz/offshorewind.html accessed in 22-3-2023.

https://www.nti-audio.com/en/support/know-how/fast-fourier-transform-fft accessed in 11/05/2023.

https://www.researchgate.net/publication/345382952_Hydro-Servo-Aero-Elastic_Analysis_of_Floating_Offshore_Wind_Turbines/citation/download/ accessed in 25-3-2023.